TRANSFORMATION INDUCED FATIGUE OF NI-RICH NITI SHAPE MEMORY ALLOY ACTUATORS

A Thesis

by

JUSTIN RYAN SCHICK

Submitted to the Office of Graduate Studies of
Texas A&M University
in partial fulfillment of the requirements for the degree of

MASTER OF SCIENCE

December 2009

Major Subject: Aerospace Engineering

TRANSFORMATION INDUCED FATIGUE OF NI-RICH NITI SHAPE MEMORY ALLOY ACTUATORS

A Thesis

by

JUSTIN RYAN SCHICK

Submitted to the Office of Graduate Studies of
Texas A&M University
in partial fulfillment of the requirements for the degree of

MASTER OF SCIENCE

Approved by:

Chair of Committee,	Dimitris C. Lagoudas
Committee Members,	Amine Benzerga
	Ibrahim Karaman
Head of Department,	Dimitris C. Lagoudas

December 2009

Major Subject: Aerospace Engineering

ABSTRACT

Transformation Induced Fatigue of
Ni-Rich NiTi Shape Memory Alloy Actuators. (December 2009)
Justin Ryan Schick, B.S., Texas A&M University
Chair of Advisory Committee: Dr. Dimitris C. Lagoudas

In this work the transformation induced fatigue of Ni-rich NiTi shape memory alloys (SMAs) was investigated. The aerospace industry is currently considering implementing SMA actuators into new applications. However, before any new applications can be put into production they must first be certified by the FAA. Part of this certification process includes the actuator fatigue life. In this study, as-received and polished flat dogbone SMA specimens underwent transformation induced fatigue testing at constant loading. The constant applied loading ranged from 100 MPa to 200 MPa. Specimens were thermally cycled through complete actuation (above A_f to below M_f) by Joule heating and environmental cooling. There were three cooling environments studied: liquid, gaseous nitrogen and vortex cooled air. It was shown that polished specimens had fatigue lives that were two to four times longer than those of as-received specimens. Test environment was also found to have an effect on fatigue life. Liquid cooling was observed to be corrosive, while the gaseous nitrogen and vortex air cooling were observed to be non-corrosive. The two non-corrosive cooling environments performed similarly with specimen fatigue lives that were twice that of specimens fatigue tested in the corrosive cooling environment. Transformation induced fatigue testing of polished specimens in a non-corrosive environment at 200 MPa had an average fatigue life of 14400 actuation cycles; at 150 MPa the average fatigue life was 20800 cycles and at 100 MPa it was 111000 cycles. For all specimens constant actuation from the beginning of testing until failure was observed, without

the need for training. Finally, a microstructural study showed that the Ni_3Ti precipitates in the material were one of the causes of crack initiation and propagation in the actuators.

To Sarah - My best friend

ACKNOWLEDGMENTS

I would first like to thank Dr. Lagoudas for giving me the opportunity to perform my master's work under his guidance. He has taught me to look critically at every problem and understand not only the math behind it, but also the application for it. Under his tutelage I have grown a great deal as an engineer. I would also like to thank Jim Mabe and Tad Calkins of The Boeing Company for their support of my project. Not only did they make it financially possible, but their technical expertise was invaluable as the project progressed. Rodney Inmon and Josh Weimar deserve my gratitude for their support in the lab; many of my test apparatuses would not have come to fruition without their hard work.

To my fellow research colleagues, Francis Phillips, Brent Volk, Krishnendu Haldar, and Darren Hartl, I owe a great deal. Some of my best learning experiences were during our technical conversations. I owe special thanks to Pariksth Kumar, from whom I learned a great deal and who was the best labmate I could ask for. I would also like to thank Olivier Bertacchini who was my mentor and collaborator on the fatigue project. Through Olivier, I learned a lot about fatigue testing and the mechanisms involved at the microstructural level. Not only did this group enhance my learning experience, but they also became my good friends.

My family and friends also deserve my gratitude. My parents, John and Sue, always encouraged me to pursue my goals. Not only did they support me with their love, but they also helped me financially and I am truly grateful. My good friends Mike Nugent, Jonathan Albritton, and Matthew Johnston have always been a good outlet of fun when I needed to get away from work, and I thank them for their support. My brothers, Josh and Jarred, whom I have had the pleasure of knowing all their lives, have always been my best friends. They have continually shown interest

in what I do and I appreciate it. Finally, I would like to thank Sarah, the love of my life and my future wife, for all the love and support she has provided me. She may not know it, but she has been my constant inspiration to perform at my best and always exceed expectations.

TABLE OF CONTENTS

CHAPTER Page

I INTRODUCTION 1
A. Fatigue of Shape Memory Alloys 2
B. Literature Review 4
C. Research Objectives and Outline of Research 6

II EXPERIMENTAL PROCEDURES 9
A. Experimental Setup 9
1. Liquid Cooling Fatigue Test Frame 10
2. Gaseous Nitrogen Cooling Fatigue Test Frame 11
3. Vortex Air Cooling 13
B. Material Selection 15
C. Test Parameters and Transformation Induced Fatigue Test Matrices 16
D. Specimen Preparation 18
E. Surface Preparation 19
F. Constant Load Transformation Induced Fatigue Testing and Data Acquisition 25

III RESULTS AND DISCUSSION 30
A. Representative Test Results 30
B. Influence of Surface Finish on Transformation Induced Fatigue 33
C. Influence of Test Environment on Transformation Induced Fatigue 36
D. Microstructural Observations 40

IV CONCLUSIONS AND FUTURE WORK 45
A. Conclusions 45
B. Future Work 47

REFERENCES 49

APPENDIX A 54

CHAPTER Page

VITA 56

LIST OF TABLES

TABLE		Page
I	Test matrix - surface effects study	17
II	Test matrix - environmental effects study	17
III	DSC measured transformation temperatures for $Ni_{60}Ti_{40}$	19
IV	Specimen cross-section dimensions for pre/post polishing	25
V	Average fatigue life of as-received vs. polished specimens	35
VI	Average fatigue life of all polished specimens	38

LIST OF FIGURES

FIGURE		Page
1	(a) SMA phase diagram, (b) pseudoelastic stress-strain plot and (c) thermal tranformation strain-temperature plot	3
2	Applied stress vs. cycles to failure for NiTiCu and equiatomic NiTi[22, 23, 24]	6
3	Strain vs. thermal cycles for (A) equiatomic NiTi actuator and (B) Ni-rich NiTi actuator[26]	7
4	Liquid cooled transformation fatigue test frame schematic	9
5	Liquid cooled transformation fatigue test frame setup	10
6	Schematic of specimen within the cooling environment	11
7	Gaseous nitrogen cooled transformation fatigue test frame schematic	12
8	(A) Gaseous nitrogen cooled transformation fatigue test frame setup, (B) a zoomed in view of the test chamber and (C) a schematic of the air circulation system	13
9	ITW Air Management vortex generator schematic	14
10	(A) Vortex air cooled transformation fatigue test frame setup and (B) a close up view of the test chamber	15
11	Dogbone test specimen geometry and dimensions	18
12	Magnified view of $Ni_{60}Ti_{40}$ oxide/recast layer	20
13	Specimen side polishing setup	21
14	Specimen test gauge side (A) before polishing and (B) after polishing	22
15	Disk polisher setup	23

FIGURE Page

16 Specimen face (A) before polishing and (B) after polishing (magnified) 24

17 Cross-sectional view of a polished specimen: (A) upper-left corner, (B) upper-right corner, (C) lower-left corner and (D) lower-right corner 26

18 Dogbone specimen in pressure grips 27

19 (A) Real-time test displacement plot and (B) breakdown of strain points per cycle 28

20 Liquid cooled transformation induced fatigue test results for (A) 200 MPa constant load, (B) 150 MPa load and (C) 100 MPa load . . 31

21 Vortex air cooled transformation induced fatigue test results for (A) 200 MPa constant load, (B) 150 MPa load and (C) 100 MPa load 32

22 Transformation induced fatigue life vs. applied stress for as-received and polished specimen tests 34

23 Fracture surfaces of (A) an as-received specimen (B) a polished specimen[31] 35

24 Polished specimen surface (A) before testing, (B) after testing in liquid and (C) after testing in gaseous nitrogen/vortex cooled air[31] 36

25 Transformation induced fatigue life vs. applied stress for all polished specimens 37

26 Actuation strain vs. applied stress for all polished specimens 39

27 Irrecoverable strain at failure for polished specimens vs. (A) applied stress and (B) cycles at failure 40

28 Characterization of precipitates using SEM[31] 41

29 Untested specimen surface and cross-section 42

30 Post-failure specimen surface 43

31 Crack initiation and propagation sites[31] 44

CHAPTER I

INTRODUCTION

Shape memory alloys (SMAs) exhibit unique thermal and mechanical properties that have been extensively studied for over fifty years. While they have been well studied, a push for industrial and commercial applications has only begun to grow in the last 15 to 20 years. The ability of SMAs to recover large strains under thermal and mechanical loading has led to the development of many applications in the biomedical, oil, and aerospace industries[1, 2, 3, 4].

To date, most SMA research has been driven by the biomedical industry and its applications, which take advantage of the pseudoelastic effect[1, 2]. The aerospace industry, on the other hand, has taken a closer look at using SMAs for thermally activated actuator applications. One of the first SMA aerospace applications that went into production was a NiTi hydraulic line coupler on the Grumman F-14[4]. The SMA coupler was cooled under stress, fitted over the hydraulic line joint and heated (under no stress) to seal the joint. More recent work has focused on taking advantage of thermally cycled SMA actuators that will be employed for many repeated actuation cycles. Examples of initial attempts to incorporate SMA actuators in aerospace applications include the DARPA Smart Wing project, which used a SMA torque tube actuator toadjust the camber of a wing, and the DARPA SAMPSON F-15 project, which used a bundle of SMA wires to rotate an inlet cowl to maximize engine efficiency[5, 6]. The Boeing Company has also been investigating using SMA torque tube and flexure beam actuators for its aerospace applications[7, 8]. Boeing

---

The journal model is *International Journal of Engineering Science*.

has focused on using Ni-rich NiTi SMA actuators due to their cyclical stability. However, before these actuators can be put into production they must be certified by the FAA, this includes the actuator fatigue life. This transformation induced fatigue life is one of the most important design factors in SMA actuators and should be thoroghly understood. To be certified by the FAA these SMA actuators must exhibit safe, consistent performance for their operational life. To date, no study has been performed on the transformation induced fatigue life of Ni-rich NiTi SMA actuators.

A. Fatigue of Shape Memory Alloys

SMAs perform work through a diffusionless, reversible transformation between the austenite and martensite phases. This phase transformation is activated when either stress and/or temperature are properly applied. When SMAs go through this phase transformation from austenite to martensite under the application of stress and/or temperature, a strain is generated; this is the transformation strain. As the SMA transforms back from martensite to austenite this transformation strain is recovered. Figure 1 (a) presents a SMA phase diagram. The two loading paths highlighted on this diagram are the two most common methods of achieving the austenite$\Leftrightarrow$martensite phase transformation. The first loading path (A) in Fig. 1 (a) is known as pseudoelastic loading, which initiates transformation by stress-inducing martensite. In pseudoelastic loading, a specimen is heated to a temperature above the austenite finish temperature (A_f) and loaded until stress induced martensite is formed. Upon unloading, the SMA returns to the austenitic phase. The corresponding stress-strain path is shown in Fig. 1 (b). The second loading path (B) shown in Fig. 1 (a) is representative of a constant stress loading path that initiates transformation by thermally inducing martensite. In this loading path, a specimen is subject to a constant

applied stress and is thermally cycled between detwinned martensite and austenite, the strain-temperature path is shown in Fig. 1 (c).

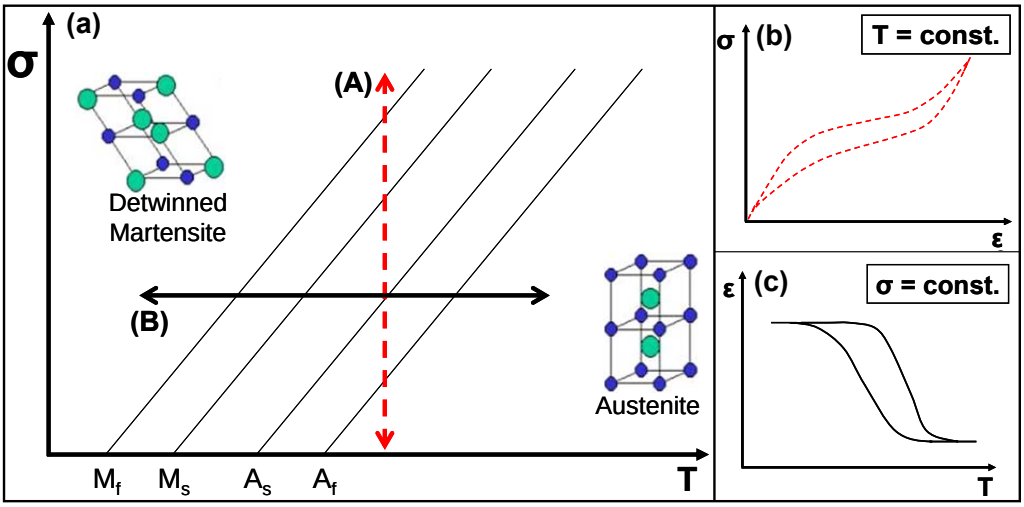

Fig. 1. (a) SMA phase diagram, (b) pseudoelastic stress-strain plot and (c) thermal tranformation strain-temperature plot

Repeating loading paths (A) or (B) leads to transformation induced fatigue of SMAs. Transformation induced fatigue is considered low cycle fatigue because it leads to the accumulation of plastic strain in the SMA, which causes failure at a low number of cycles (10^4-10^5 cycles)[9]. As long as transformation is induced, both loading paths exhibit this behavior. However, the pseudoelastic loading path is not relevant for SMA actuator applications, so transformation induced fatigue testing for actuators needs to by done through loading path (B). It should be noted that SMAs do exhibit high cycle fatigue similar to that of conventional metals, as long as no phase transformation is induced.

B. Literature Review

The first fatigue study of NiTi SMAs was performed by Melton and Mercier in 1978, when pseudoelastic fatigue tests were run on wire specimens with different martensite start temperatures[10]. This work was soon followed by that of McNichols and Brookes, who studied the fatigue life of NiTi pseudoelastic springs. It wasn't until the early '90s, when the medical industry began to push for less invasive medical procedures, that more focus was placed on the high cycle fatigue of SMAs. Equiatomic NiTi, with its pseudoelastic effect, was found to have several ideal properties for less invasive medical devices[2]. More needed to be understood on the high cycle fatigue life of NiTi SMAs before they could be widely used in medical applications. A great deal of pseudoelastic fatigue work was done by Tobushi and co-workers; they used rotating-bending fatigue of wires to strain induce a phase transformation in both tension and compression[11, 12, 13, 14]. In this series of works it was found that, if the amount of applied stress/strain was low enough, only a rhombohedral-phase (R-phase) transformation was induced and the SMAs would exhibit high cycle fatigue ($>10^7$ cycles), however if a full phase transformation from austenite to martensite was induced then low cycle fatigue was exhibited by the SMAs ($<10^(3)$ cycles). Pelton, Gong and Duerig then performed fatigue tests on stent-like structures and found that the actual application fatigue matched well with wire fatigue results from the work done by Tobushi[15]. A work done on the pseudoelastic fatigue response of dental drills also showed similar fatigue results to that of Tobushi and co-workers[16]. Another pseudoelastic application that has been recently investigated is vibrational damping[17, 18, 19, 20]. While SMAs show potential for damping applications, their fatigue life of 10^5 was closer to low cycle fatigue life and is two orders of magnitude lower than what most damping applications will require (10^7 cycles).

More recently the aerospace industry has begun to investigate how to use thermally activated SMA actuators in future aircraft designs[5, 6, 7, 8, 21]. In these initial works equiatomic NiTi has been studied as a potential actuator. The focus has primarly been on characterizing the material for actuator design, including determining the optimal material preparation, determining the number cycles to stabilization and the actuation strain under various applied loads. However, these works fail to address the transformation induced fatigue of the material. There have been few studies on the transformation induced fatigue of NiTi actuators; one of the first was by Proft, Melton and Duerig[22]. In this work the actuator properties of NiTi and NiTiCu were compared, including fatigue life. From their initial work it was found that NiTiCu, with its smaller thermal hysteresis, would make a better actuator material. This led to more in-depth research on NiTiCu and its cyclical properties. David Miller performed some of the first transformation induced fatigue testing of SMA actuators at Texas A&M[23]. In this study an optimal heat treatment for the NiTiCu wire actuators was determined and then fatigue tests were performed for partial and complete actuation. Olivier Bertacchini then studied partial and complete transformation cycles of NiTiCu wires[24]. From this work it was shown that partial transformation cycling resulted in longer fatigue lives than complete transformation cycling. The transformation induced fatigue life versus the applied stress results for Proft et al., Miller and Bertacchini are shown in Fig. 2.

However,De Araujo, Morin and Guenin studied actuation strain and accumulated plastic strain versus applied stress of NiTiCu actuators and found that the actuator properties degrated at higher applied stresses[25]. This study showed that at constant applied loads of 175 MPa or more the properties of the NiTiCu wire actuators were altered (actuation strain went down, accumulated plastic strain went up). Similar results were found for equiatomic NiTi SMA actuators, where they were less cycli-

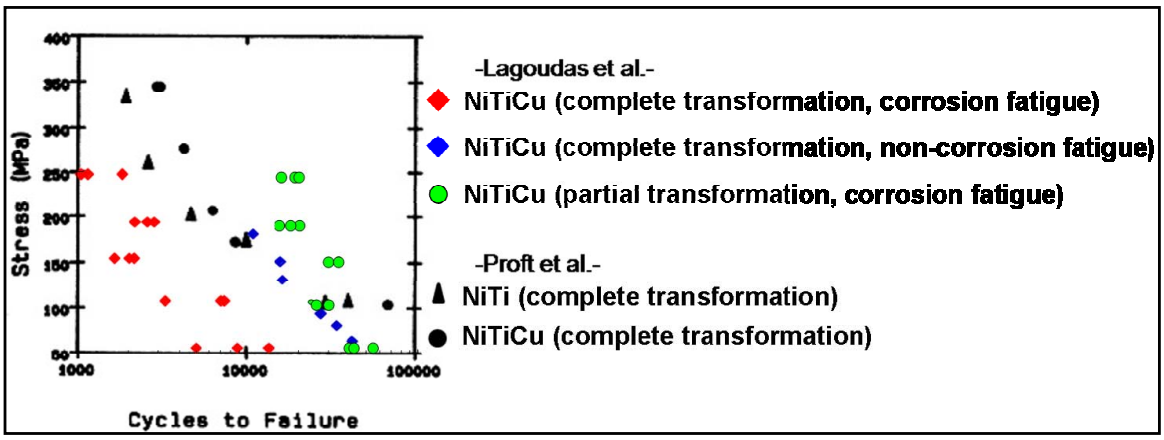

Fig. 2. Applied stress vs. cycles to failure for NiTiCu and equiatomic NiTi[22, 23, 24]

cally stable at higher applied stresses, this is shown in Fig. 3 (A)[26]. From these studies it was found that while NiTiCu and equiatomic NiTi are capable actuators, they tend to develop large amounts of plastic strain under higher loads. Also, as accumulated plastic strain increases over cycles, the actuation strain decreases. From these results, studies were performed to improve the stability of SMA actuators with techniques such as precipitate hardening[27, 28, 29]. It was found that Ni-rich NiTi has precipitates in it that can improve material properties, including stabilization of the actuation strain and limiting the accumulation of plastic strain, this is shown in Fig. 3 (B). No studies have yet been performed on the transformation induced fatigue of Ni-rich NiTi SMA actuators.

C. Research Objectives and Outline of Research

It can be seen from the literature review that there has no work done on the transformation induced fatigue of Ni-rich NiTi SMAs. Aerospace companies are exploring using SMAs in thermally activated actuator applications, and Ni-rich SMAs are being

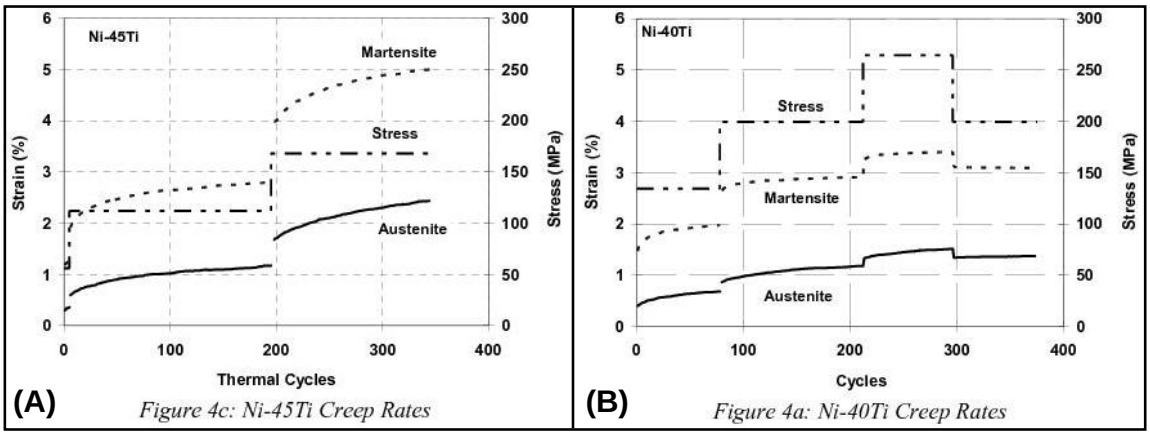

Fig. 3. Strain vs. thermal cycles for (A) equiatomic NiTi actuator and (B) Ni-rich NiTi actuator[26]

studied in particular due to their stable cyclic performance. While previous works have studied the cyclic properties of Ni-rich SMA actuators, actuators were never tested until failure. As a result, the main objective of this study is to conduct transformation induced fatigue experiments for Ni-rich SMA actuators. In particular, the Ni-rich SMA to be studied will be $Ni_{60}Ti_{40}$ (wt.%) ($Ni_{55}Ti_{45}$ (at.%)). This material was chosen because it is currently being studied by the aerospace industry for use in SMA actuator applications.

For this study, the actuators to be used will be flat dogbone specimens. Thermal cycling of these SMA actuators involves heating and cooling the actuators under stress to induce the phase transformation. Test specimens will undergo complete transformation cycling (100% austenite $\Leftrightarrow$ 100% martensite), while being subjected to constant loading. To do this, all fatigue tests will be performed in an environment that will be cooled below the SMA's M_f temperature, while Joule resistive heating will be used to bring the specimen temperature above A_f. Two separate test frames will be used to implement different cooling environments. One test frame will cool

specimens by forced-convection with a circulating liquid bath of chilled ethylene-glycol. The second test frame will use forced-convection of gaseous nitrogen, and later vortex cooled air, to cool the specimens. A LabView program will be used to control all tests and record all experimental data.

In Chapter II, the experimental setup and procedure will be described in detail. A description of the two test frames used for this study will first be provided. Following this, discussion will be provided on material selection and specimen preparation. An in-depth description of the test procedure will then be given. Finally, the test matrix and parameters to be studied will be detailed.

Chapter III will provide the fatigue testing experimental results and discussion. A representative test result will be presented and discussed. Then, the results for polished and as-received specimens will be described and analyzed to determine the effects of surface finish on fatigue life. Next, the effects of environment for specimens cooled with liquid, specimens cooled with gaseous nitrogen and specimens cooled with vortex cooled air will be compared. Additional discussions will be made regarding analysis of the actuation strain versus applied stress and the irrecoverable strain at failure versus applied stress and cycles at failure. Finally, a study on the impacts of microstructure will be presented.

CHAPTER II

EXPERIMENTAL PROCEDURES

In Chapter I, a general introduction to SMAs and the fatigue of SMAs was given. The current chapter will describe the experimental setup for fatigue testing as performed in this study. This will include the details of the test setup, specimen preparation, testing procedure, test parameters and fatigue test matrices.

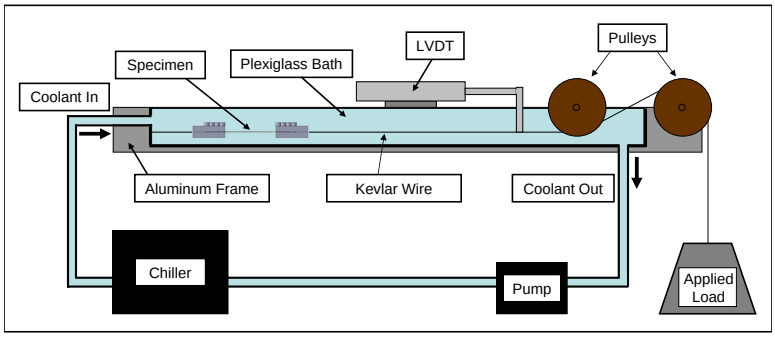

Fig. 4. Liquid cooled transformation fatigue test frame schematic

A. Experimental Setup

Two test frames have been developed and built at Texas A&M for the purpose of performing transformation induced fatigue testing. While both test frames have similar capabilities, they differ in the methods used to cool the specimens during testing. The first test frame described has been used in previous studies[24, 30] and provides forced fluid convection cooling with ethylene-glycol. The second test frame was designed and built to perform comparably to the first, except that it implemented forced gaseous nitrogen convection cooling, which was later replaced by vortex air cooling.

These new cooling methods were implemented to reduce the possibility of a corrosive environment during fatigue testing. The test frames are discussed in detail in the following sections.

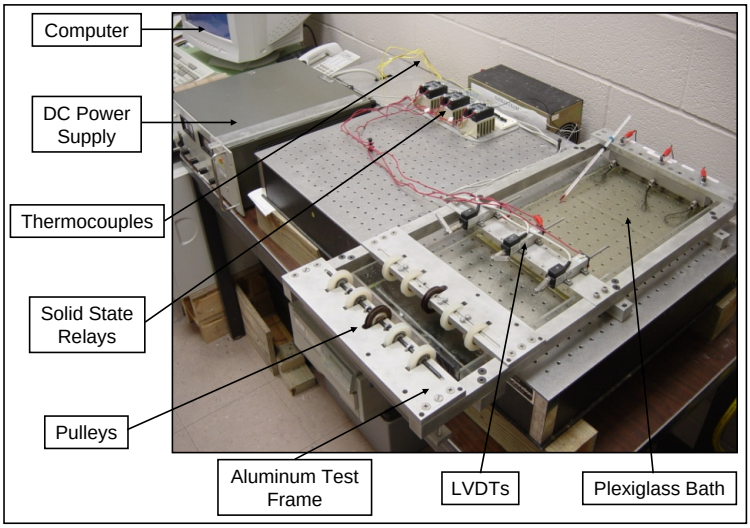

Fig. 5. Liquid cooled transformation fatigue test frame setup

1. Liquid Cooling Fatigue Test Frame

A schematic of the first test frame is presented in Fig. 4 and an actual view of the test setup is shown in Fig. 5. An aluminum test frame surrounds a plexiglass bath containing a circulating chilled liquid (ethylene-glycol). The liquid ethylene-glycol is cooled to 5°C (41°F) by a Kreonite water cooler and circulated through the plexiglass bath by a pump system. The aluminum frame has fix points in the back to secure the specimens in place during testing. The front of the frame has pulleys to redirect the applied load so that it is in line with the specimens. The pulleys are on bearings to minimize friction. Linear variable displacement transducers (LVDTs) with 55 mm (2.17 in.) action arms are used to measure displacements during testing.

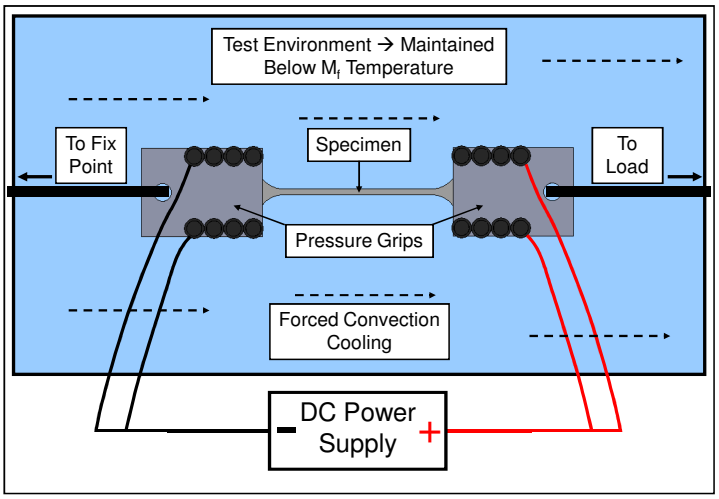

Fig. 6. Schematic of specimen within the cooling environment

Thermocouples are used to monitor the bath during testing and ensure the cooling is consistent throughout testing. Kevlar ropes are used to connect the specimen to the fix point, LVDT, and applied load. A Hewlett-Packard 6261B DC power supply is used to resistively heat the specimen, and NTE Electronics solid state relays are used to control when the resistive heating takes place. A schematic of the specimen in the test setup, connected to the DC power supply, the fix point and the applied load is presented in Fig. 6. LabView is used to control the test and collect data through a National Instruments PCI-6035E DAQ card.

2. Gaseous Nitrogen Cooling Fatigue Test Frame

It was observed that testing in the liquid cooled environment left a residue on the surface of the tested specimens and it was determined that this residue could be a sign of a mildly corrosive environment. Therefore, a second frame was developed and built at Texas A&M to use a less corrosive cooling environment.

A schematic of the new test frame is shown in Fig. 7 and an actual picture of

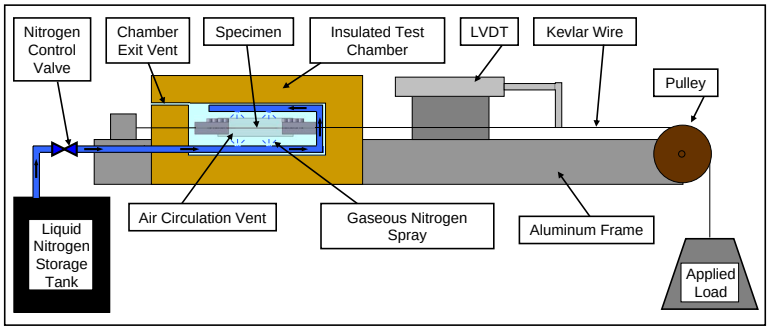

Fig. 7. Gaseous nitrogen cooled transformation fatigue test frame schematic

the setup is shown in Fig. 8 (A). The selected cooling medium was gaseous nitrogen, which allows for a much colder and dry testing environment (-15°C vs. 5°C in the liquid cooled test frame). Another advantage of the gaseous nitrogen cooling system is that nitrogen is stored at high pressure and when it is sprayed into the test chamber it creates a positive pressure which drives out any moisture in the chamber. As a result, the gaseous nitrogen cooling system creates an environment that is corrosion free. Liquid nitrogen is stored in large dewars (240 L) at high pressure (1.55 MPa) and is released by a LabView controlled cryogenic solenoid valve when needed. As the liquid nitrogen expands into gas, it is sprayed into a 51 mm x 51 mm x 127 mm (2 in. x 2 in. x 5 in.) insulated chamber, a zoomed in view of the test chamber is shown in Fig. 8 (B). The test specimen and grips are contained within this chamber. There are holes at both ends of the chamber to allow for the kevlar rope to extend out and connect the specimen to the fix point, LVDT, and applied load. An air circulation system allows for even and efficient forced convection cooling of the specimen in the chamber, this is shown in Fig. 8 (C). One thermocouple was placed in the chamber to monitor the temperature during testing. The chamber temperature was set to be -15°C (5°F) during testing. The gaseous nitrogen chamber was kept at a colder

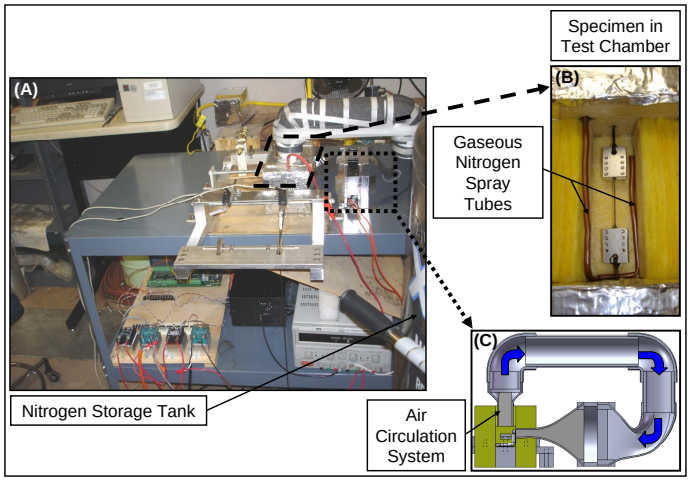

Fig. 8. (A) Gaseous nitrogen cooled transformation fatigue test frame setup, (B) a zoomed in view of the test chamber and (C) a schematic of the air circulation system

temperature (-15°C) than the liquid environment (5°C) to compensate for the reduced heat transfer capability of gaseous cooling. Thus, comparable fatigue cycle rates could be maintained between the two test frames.

3. Vortex Air Cooling

To perform fatigue testing in the gaseous nitrogen cooled test frame was costly and time consuming to maintain. One liquid nitrogen dewar stores enough gas for roughly twenty-four hours of testing. With tests that last days at a time, it was logistically difficult and expensive to swap tanks in and out daily without disrupting testing. Another issue was the cryo-valve that controlled when the nitrogen was released into the chamber. The valve was only rated for a certain number of open-close actuations and would often malfunction during testing. To reduce cost and eliminate any disruptions during testing a new form of cooling was implemented that achieved the same non-corrosive results as the gaseous nitrogen.

This new test setup is identical to the gaseous nitrogen test setup except for the cooling method. The new cooling method chosen was vortex air cooling. Vortex generators work by taking compressed air and forcing it into a vortex. This vortex is then separated into hot and cold flows which are vented out at the opposite ends of the generator. The cold flow from the vortex generator is vented into the test chamber for forced convection cooling. A schematic of the vortex generator is shown in Fig. 9. All vortex generators used for this setup were acquired from ITW Air Management.

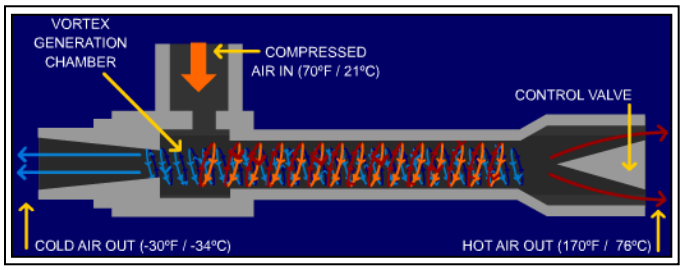

Fig. 9. ITW Air Management vortex generator schematic

There are several distinct advantages of the vortex cooling. The vortex generators are easy to maintain and can run without interruption, as long as compressed air is continuously applied. Compared to gaseous nitrogen the vortex setup is much cheaper to maintain and run. Finally, the vortex cooling can achieve temperatures of -12°C to -15°C and create a very turbulent environment for forced convection cooling. The final vortex cooled air test frame is shown in Fig. 10. To prevent any moisture from entering the test, an air dryer was added to the compressed air line before it enters the vortex generators to eliminate moisture in the chamber. A plexiglass chamber enclosing the entire test frame was added to eliminate any moisture buildup on the outside of the test chamber.

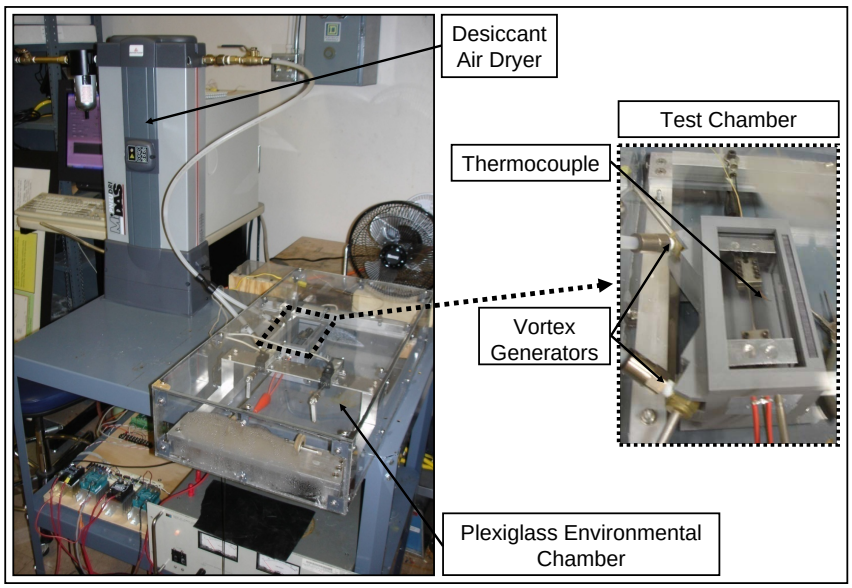

Fig. 10. (A) Vortex air cooled transformation fatigue test frame setup and (B) a close up view of the test chamber

B. Material Selection

The selected material for this study is $Ni_{60}Ti_{40}$ (wt.%) ($Ni_{55}Ti_{45}$ (at.%)). It is one of the Ni-rich NiTi SMA materials currently being studied for actuator use in the aerospace industry because of its stable actuation response, even under increased loading[26]. Also, by performing an aging heat treatment the transformation temperatures of this material can be tailored for specific application needs. An initial characterization of this material was conducted at Texas A&M and led to the determination of the optimal nickle content, heat treatment and specimen size that was used in this study[31]. The heat treatment and specimen size will be discussed in detail in the section on specimen preparation.

C. Test Parameters and Transformation Induced Fatigue Test Matrices

In this study all specimens will undergo transformation induced fatigue for complete actuation cycling. Tests will be conducted at constant stress levels of 100 MPa (14.5 ksi), 150 MPa (21.75 ksi) and 200 MPa (29.0 ksi) based on the level of stress that SMA actuators are going to see in the applications mentioned in the introduction. First, the effects of surface finish on the transformation induced fatigue life will be examined. As-received specimens and polished specimens will be tested in the liquid cooling fatigue test frame and the results compared; this test matrix is shown in Table I. Next, the effects of environment on actuator performance and transformation induced fatigue life will be studied. Polished specimens will undergo transformation induced fatigue testing in the gaseous nitrogen cooled environment, the vortex air cooled environment and the liquid cooled environment and the results will be compared. The actuation strain versus applied stress and the total irrecoverable strain versus applied stress and cycles at failure will also be compared for all polished specimens. The test matrix for the gaseous nitrogen and the vortex cooled air fatigue tests is shown in Table II.

Table I. Test matrix - surface effects study

Material	Test Environment	Surface Finish	Applied Stress MPa (ksi)	Number of Tests
$Ni_{60}Ti_{40}$	Liquid	As-Received	100 (14.50)	4
			150/21.75	4
			200 (29.00)	4
$Ni_{60}Ti_{40}$	Liquid	Polished	100 (14.50)	4
			150/21.75	4
			200 (29.00)	4

Table II. Test matrix - environmental effects study

Material	Test Environment	Surface Finish	Applied Stress MPa (ksi)	Number of Tests
$Ni_{60}Ti_{40}$	Gaseous Nitrogen	Polished	100 (14.50)	–
			150/21.75	4
			200 (29.00)	4
$Ni_{60}Ti_{40}$	Vortex Cooled Air	Polished	100 (14.50)	2
			150/21.75	3
			200 (29.00)	3

D. Specimen Preparation

Flat dogbone shaped specimens were used in this study. Dogbone actuators were chosen, as opposed to wire actuators, because for transformation induced fatigue testing they were easier to grip without creating any hot spots or stress concentrations in the grips. Also, specimens were cut from large rectangular beam actuators and to represent a similar cross-section during testing the specimens were cut as flat dogbones. The specimen dimensions were dictated by two factors. The test frame in

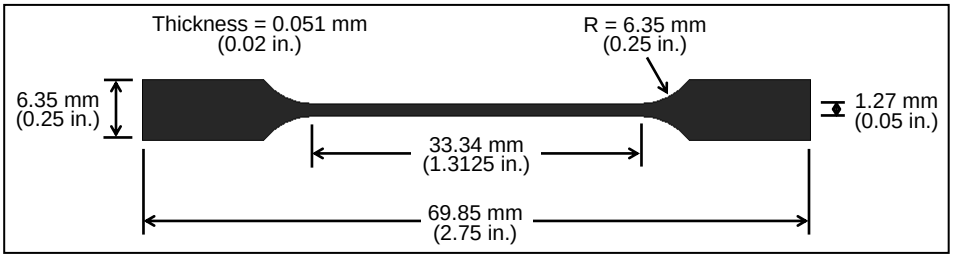

Fig. 11. Dogbone test specimen geometry and dimensions

use was initially designed for small wire fatigue testing and therefore had load limit restrictions. More importantly, one goal of this study was to perform transformation induced fatigue testing quickly. In order to perform fatigue testing in a time frame of days or weeks instead of months or years, the specimens needed to be small enough to allow for rapid heat transfer. The faster heat can be added or removed from the system, the quicker cycle times become. Specimen dimensions are shown in Fig. 11. All specimens were accurately cut to the proper dimensions using electro discharge machining (EDM).

A two stage heat treatment process was then performed on the $Ni_{60}Ti_{40}$ dogbones. The first stage was a shape setting heat treatment of 1 hour at 850°C (1562°F) in a

vacuum, followed by furnace cooling. The second stage was an aging heat treatment at 450°C (842°F) for 20 hours followed by water quenching. By performing this two stage heat treatment the transformation temperatures were optimized for the testing capabilities of the fatigue test frames used in this study. The transformation temperatures at zero-stress were measured by differential scanning calorimetry (DSC) and are summarized in Table III.

Table III. DSC measured transformation temperatures for $Ni_{60}Ti_{40}$

M_s=24°C (75°F)	A_s=48°C (118°F)
M_f=20°C (68°F)	A_f=59°C (138°F)

E. Surface Preparation

In the initial parametric study, specimens were cut by the waterjet method[31]. This method was quickly abandoned as the test gauge cuts were observed to be irregular. EDM was found to cut a more accurate test gauge and was used for all specimens tested in the current study. The EDM method removes material by creating electro-discharges between the working tool, usually copper, and the material work-piece. The process vaporizes small amounts of material from the work-piece, which are removed by the liquid dielectric in which the EDM process takes place. A "recast" layer was developed along the surface of the material where it was cut by the electro-discharging[32]. It was found that the material on the surface was first super-heated by the cutting and then super-cooled by the liquid dielectric. This created a rough surface that was covered in a recast layer of craters and cracks, see Fig. 12. The cracks were created to relieve stress in the brittle recast layer when it was rapidly cooled. The recast layer was found to be extremely Ni-rich and the oxide layer was

found to be Ti-rich, consisting primarily of TiO_2 and $TiNiO_3$. A magnified view of an EDM cut specimen is shown in Fig. 12. The measured depth of this oxide/Ni-rich

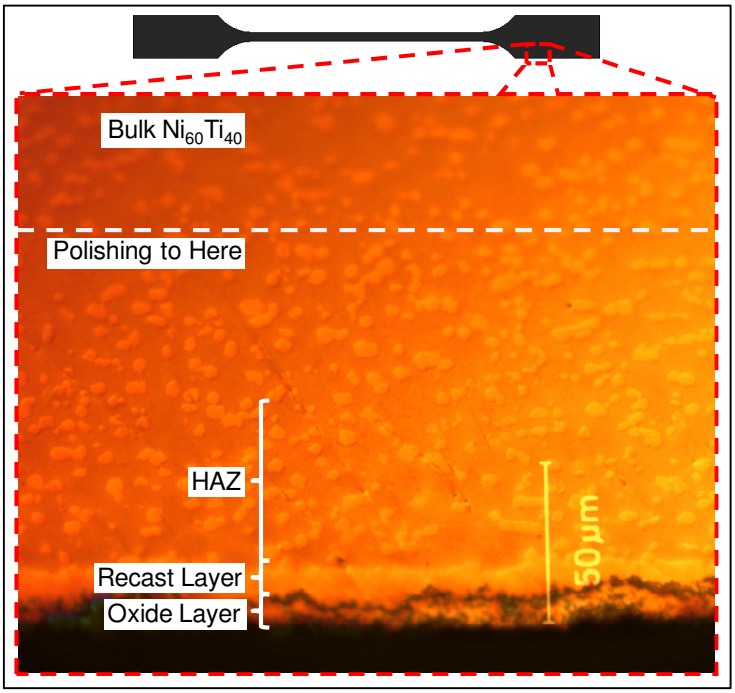

Fig. 12. Magnified view of $Ni_{60}Ti_{40}$ oxide/recast layer

recast layer was found to be 15-25 μm (0.4-1.0x10^{-3} in.). Due to the extreme changes in temperature, the material near the surface develops a "heat affected zone" (HAZ) that is measured to reach a depth of 51 μm (2.0x10^{-3} in.) beyond the recast layer[33]. This heat affected zone must also be accounted for when preparing the specimens for testing, as there could have been some microstructural changes to the material due to the extreme temperature changes. It is necessary to removed these damaged layers, so that the bulk fatigue properties of $Ni_{60}Ti_{40}$ can be accurately predicted.

A few polishing methods were explored, including electropolishing, sand blast-

ing and mechanical polishing. It was difficult to achieve an even polish when using electropolishing on the rectangular cross-section of such small specimens. Also, electropolishing was found to round-off the rectangular cross-section corners. The specimen's small size also eliminated sand blasting as an effective polishing method. Through this process of elimination, mechanical polishing was chosen to remove the damaged material from all specimens prior to testing. A reliable and repeatable mechanical polishing process was developed to remove 127 μm (5.0x10^{-3} in.) from all test gauge surfaces. Removing the damaged material will ensure that the oxide layer, the recast layer and the heat affected zone, a total of 76 μm (3.0x10^{-3} in.), would be removed. An extra 51 μm (2.0x10^{-3} in.) was also removed to ensure that the undamaged bulk material was reached.

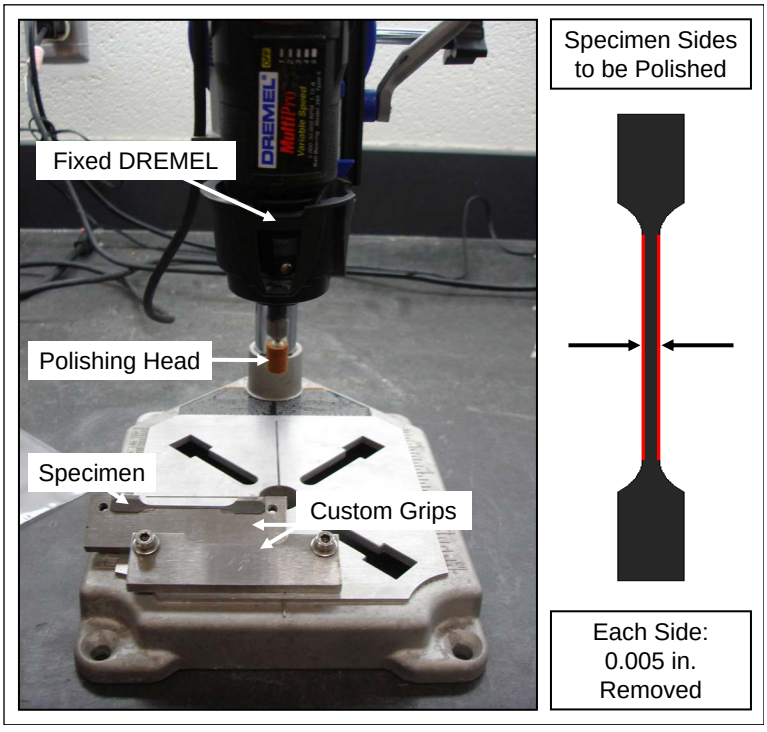

Fig. 13. Specimen side polishing setup

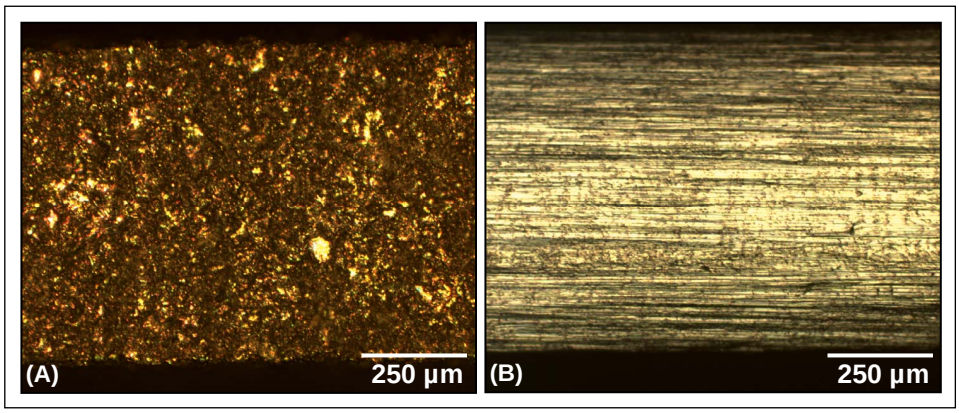

Fig. 14. Specimen test gauge side (A) before polishing and (B) after polishing

The first stage in the polishing process was to polish the sides of the specimen test gauge. A variable-speed DREMEL grinder was used to perform this task. The DREMEL grinder was fixed into a stand to ensure that it always remained perpendicular to the specimen surface. A specimen was then placed into custom grips that only allowed 127 μm (5.0x10^{-3} in.) of the test gauge to protrude. The Dremel setup and the custom grips can be seen in Fig. 13. The first 102 μm (4.0x10^{-3} in.) of material were removed with a DREMEL 3/8 inch aluminum oxide grinding stone and the final 25 μm (1.0x10^{-3} in.) were removed with a fine-finish 3/32 inch, 400-grit rubber polishing bob. During all DREMEL polishes, the specimen was continuously sprayed with water to remove any free material and to cool the specimen. Moving the exposed surface of the entire test gauge of the specimen back and forth along the polishing head was done by hand in slow, repeatable motions that applied a minimal amount of force. Figure 14 shows the side of a specimen before and after polishing. It is noted that grooves remain from the final polish on the specimen sides. This was a result of the fact that the finest polishing bob that could be acquired for the DREMEL was as 400-grit polishing bob. These grooves were found to be inconsequential to the fatigue

life. There are two primary reasons for this assumption. The first is that the grooves run parallel to the applied stress, which makes them less likely to induce cracking. Secondly, as will be shown in the results, all polished specimen failures were found to initiate from the specimen face surfaces and not the specimen side surfaces.

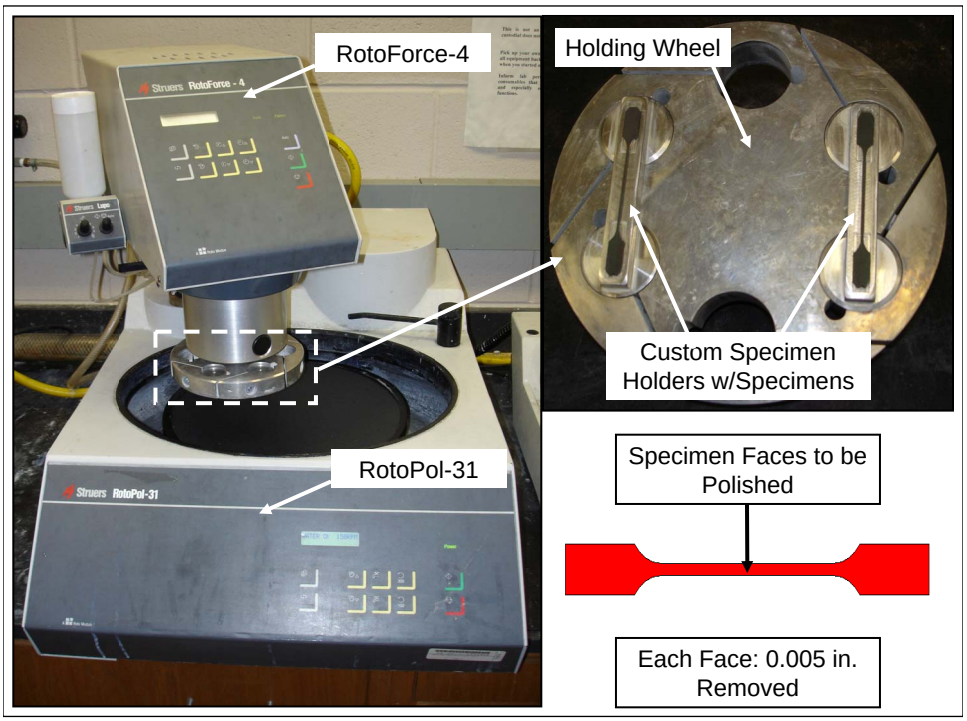

Fig. 15. Disk polisher setup

The specimen faces were polished next. Figure 15 presents a picture of the face polishing setup. A custom holder was developed that fixes the specimen in place during polishing and prevents any bending or twisting of the specimens. The specimen was placed into this holder, which was then placed into a large specimen holding wheel for polishing. Two specimens can be properly polished in this holding wheel at a time. The holding wheel was then attached to a Struers RotoForce-4 polishing control arm.

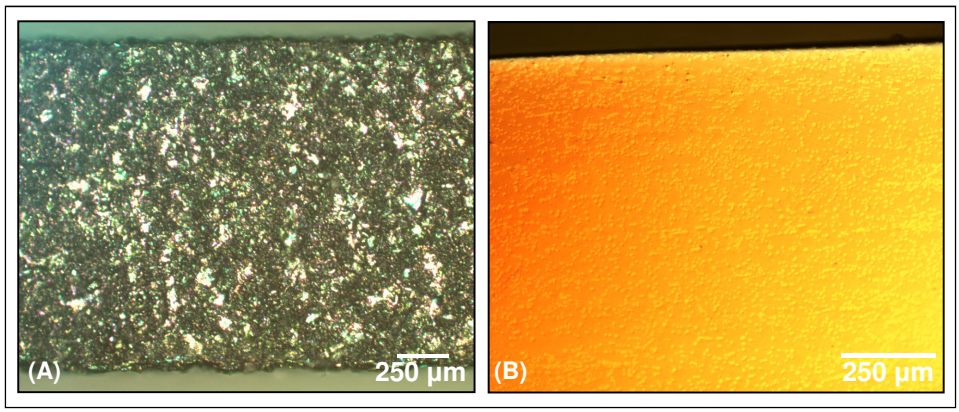

Fig. 16. Specimen face (A) before polishing and (B) after polishing (magnified)

The RotoForce-4 can control both the direction, applied force and the polishing time on the specimens to ensure proper polishing process repeatability. For all polishing on the RotoForce-4, a minimum force of 5 N was applied. The specimens were polished with a Struers RotoPol-31, which contains the polishing disk and controls grinding speed. 102 μm (4.0x10^{-3} in.) was first ground off using a 400-grit polishing disk. This was followed by a step up to 1200-grit and then 2000-grit, which removed another 25 μm (1.0x10^{-3} in.) from each face. Finally, the specimens were given a mirror quality finish with a 0.3 micron polishing solution. This finish ensures that there are a minimum number of possible initiation points from which fatigue cracks can progagate and that these small specimens can properly predict bulk material fatigue properties. The as-received specimen face compared to the final polished face can be seen in Fig. 16. A detailed step-by-step polishing procedure for both specimen sides and faces is included in Appendix A.

Specimens that were polished were EDM cut to have an initial test gauge cross-section of 0.76 mm (0.03 in.) thick by 1.52 mm (0.06 in.) wide. By oversizing the specimens, 127 μm (5.0x10^{-3} in.) was removed from all faces and a damage free cross-

section of 0.51 mm x 1.27 mm (0.02 inches x 0.05 inches) was achieved. Table IV presents a comparison between the average test gauge width and thickness of the specimens as-received and polished. The final thickness and width of the polished

Table IV. Specimen cross-section dimensions for pre/post polishing

	As-Received	Polished
Average Width	1.529 ± 0.025 mm (0.060 ± 0.001 in.)	1.242 ± 0.051 mm (0.049 ± 0.002 in.)
Average Thickness	0.747 ± 0.000 mm (0.029 ± 0.000 in.)	0.462 ± 0.025 mm (0.018 ± 0.001 in.)

test gauges are slightly below the target of 0.51 mm x 1.27 mm. However, the goal of removing at least 127 μm from all sides was achieved and all damaged material was removed from the specimens. In Fig. 17, the cross-sectional view of a polished, untested specimen can be seen. When compared to Fig. 12, it can be seen that the oxide/recast layers have been removed from all sides of the test gauge. Also, it can be observed that all surfaces of the cross-section are smooth, thus illustrating the quality of the finish created by the polishing.

F. Constant Load Transformation Induced Fatigue Testing and Data Acquisition

In this study the tests were designed to achieve complete thermal transformation of the specimens. Specimens were placed into the test frame and fixed at one end to the fix-point on the test frame by kevlar ropes. The other end was connected to the LVDT and the constant applied load with another kevlar rope. The power source providing the Joule heating was then connected to the steel specimen grips by way of

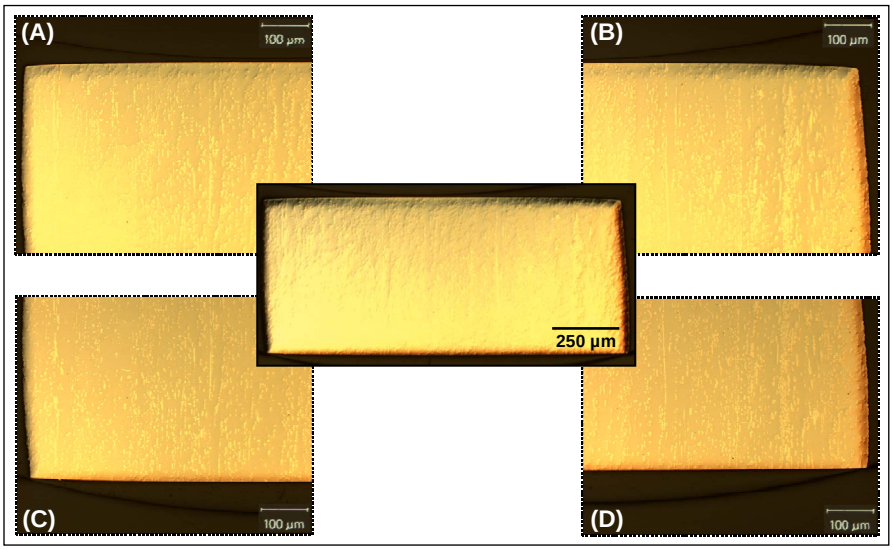

Fig. 17. Cross-sectional view of a polished specimen: (A) upper-left corner, (B) upper-right corner, (C) lower-left corner and (D) lower-right corner

small wires that would not interfere with specimen actuation. A picture of a specimen in pressure grips is presented in Fig. 18.

LabView control program was then activated and the environment surrounding the specimen was brought down to the desired temperature (5°C for the liquid cooling, -15°C for the gaseous nitrogen/vortex cooling). At that point the specimen had been cooled below the martensite finish temperature and, due to the applied load, underwent detwinning. Specimen thermal cycling was then started and continued until specimen failure.

Since it is not feasible to place a thermocouple on a specimen during testing, LVDT displacement measurements were used to ensure complete actuation was achieved during thermal cycling. All tests were performed under time controlled cycles, with a set amount of time for heating and for cooling. Before any fatigue testing was performed, several calibration tests were run to determine the proper heating and

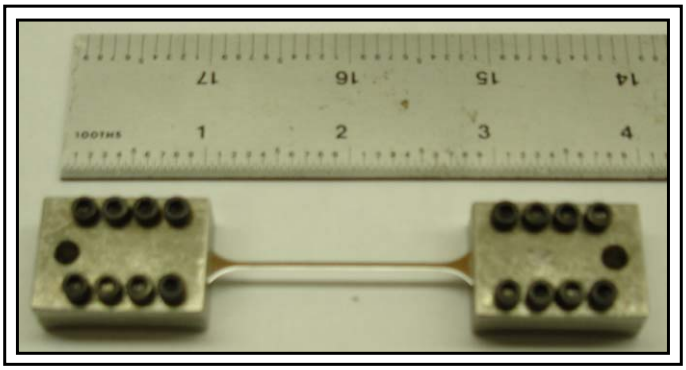

Fig. 18. Dogbone specimen in pressure grips

cooling times needed to achieve complete actuation (100% austenite ⇔100% martensite). Calibrations were performed for each of the constant load levels in each of the test environments studied in this work. This was done by heating the specimen until it was measured by thermocouples to be above A_f and no change in displacement was measured by the LVDT and then allowing the test environment to cool the specimen until the thermocouples showed that the specimen was below M_f and there was no measured change in displacement. Generally, 1-3 seconds of heating were needed to bring the specimens above the A_f temperature, with an average of 2.5 volts and 22 amps applied. For cooling, 7-9 seconds were needed for the cooling environment to bring specimens below the M_f temperature. Two position data points were taken over each cycle, one at the end of heating (austenite position) and one at the end of cooling (martensite position). A real-time displacement plot of one cycle from a transformation induced fatigue test is shown in Fig. 19 (A), with the red square being the measured austenite position and the blue circle being the measured martensite position. Given that the LVDTs only measure position, each set of test data must be rescaled by the first-cycle measured austenite position and then normalized into

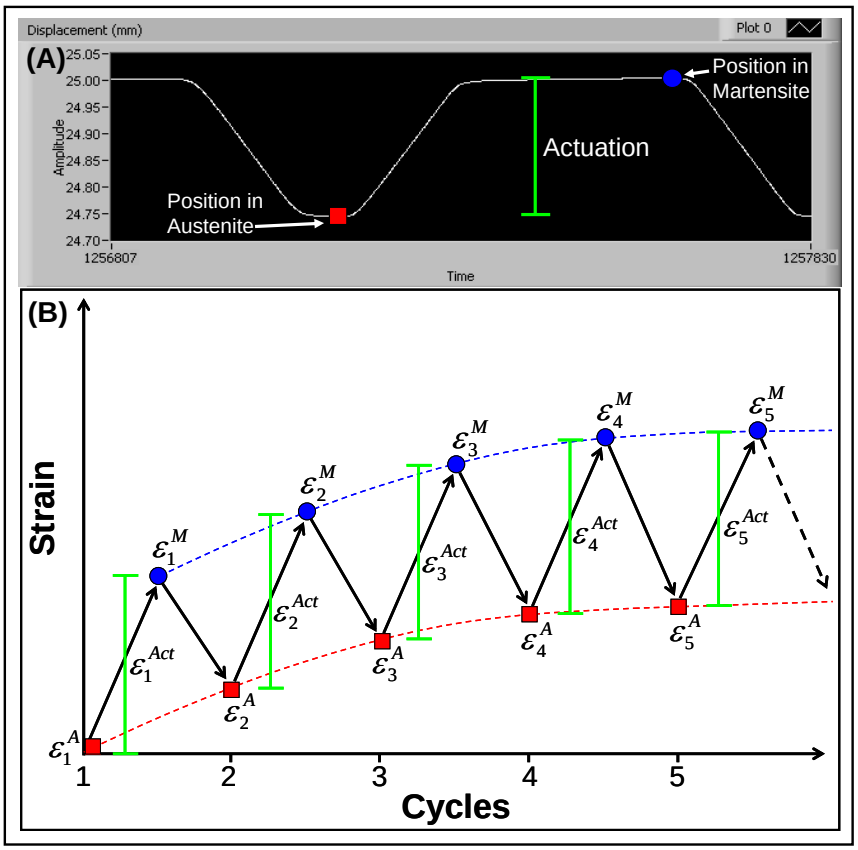

Fig. 19. (A) Real-time test displacement plot and (B) breakdown of strain points per cycle

strain measurements by the following equations:

$$\varepsilon_i^A = \frac{l_i^A - l_1^A}{L_0} \tag{2.1}$$

$$\varepsilon_i^M = \frac{l_i^M - l_1^A}{L_0}. \tag{2.2}$$

Where ε^A is the strain in austenite, ε^M is the strain in martensite, l is the LVDT measured position, L_0 is the test gauge length and i is the cycle number. Figure 19 (B) shows a cyclic breakdown of the strains for austenite and martensite. The actuation

strain (ε^{Act}) for each cycle was calculated by

$$\varepsilon_i^{Act} = \varepsilon_i^M - \varepsilon_i^A. \tag{2.3}$$

The total irrecoverable strain (ε^I) at each cycle can also be calculated. Because the austenitic displacement measurement from the first cycle was used to rescale all data, all elastic strains in the system (kevlar ropes, austenite response) were already taken into account. This can be assumed because the applied stress on the actuator is constant, thus the elastic strain is constant. The following equation was used to calculate the total irrecoverable strain at each cycle until failure.

$$\varepsilon_i^I = \frac{l_i^A - l_1^A}{L_0} \tag{2.4}$$

CHAPTER III

RESULTS AND DISCUSSION

In this chapter the data collected from the tests described in Chapter 2 will be presented and discussed. A representative test result will be shown and described in the first section. Then, in the second section, the effects of surface finish on the fatigue life will be studied. In the third section, the effects of environment on fatigue life and actuator performance will be considered. The actuator performance relations discussed in section two include the actuation strain compared to the applied stress level and the irrecoverable strain at actuator failure compared to applied stress level and cycles at failure. Finally, a brief discussion on microstructure and its effects on the transformation induced fatigue will be presented in the fourth section.

A. Representative Test Results

As previously described, each fatigue test collects two displacement points per thermal cycle, one in the austenite phase and one in the martensite phase. This is performed at every cycle for the length of the test. Strains are then calculated from the displacements and plotted versus test cycles. A set of representative test results from the liquid cooled transformation induced fatigue test frame is shown in Fig. 20. Figure 21 then presents a set of vortex cooled transformation induced fatigue test results. All test results presented were tested under constant loading, performed complete actuation cycles, and were cycled until failure. The three plotted curves in each result represent the strain in martensite (ε^M, blue curve), strain in austenite (ε^A, red curve), and the actuation strain (ε^{Act}, green curve). The martensitic strain

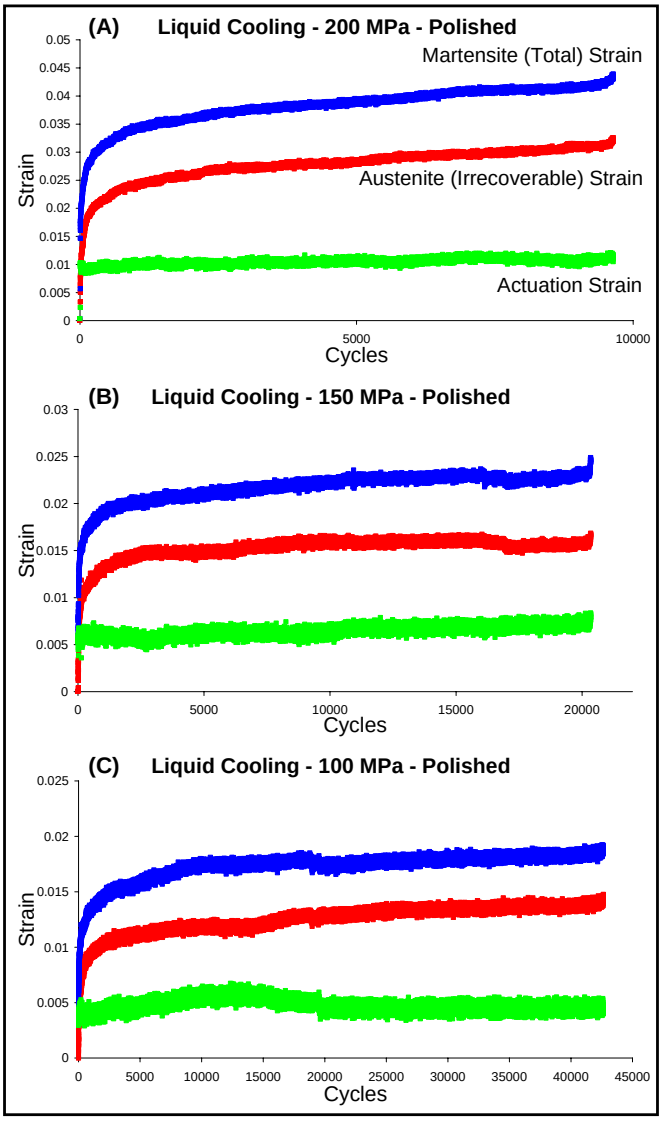

Fig. 20. Liquid cooled transformation induced fatigue test results for (A) 200 MPa constant load, (B) 150 MPa load and (C) 100 MPa load

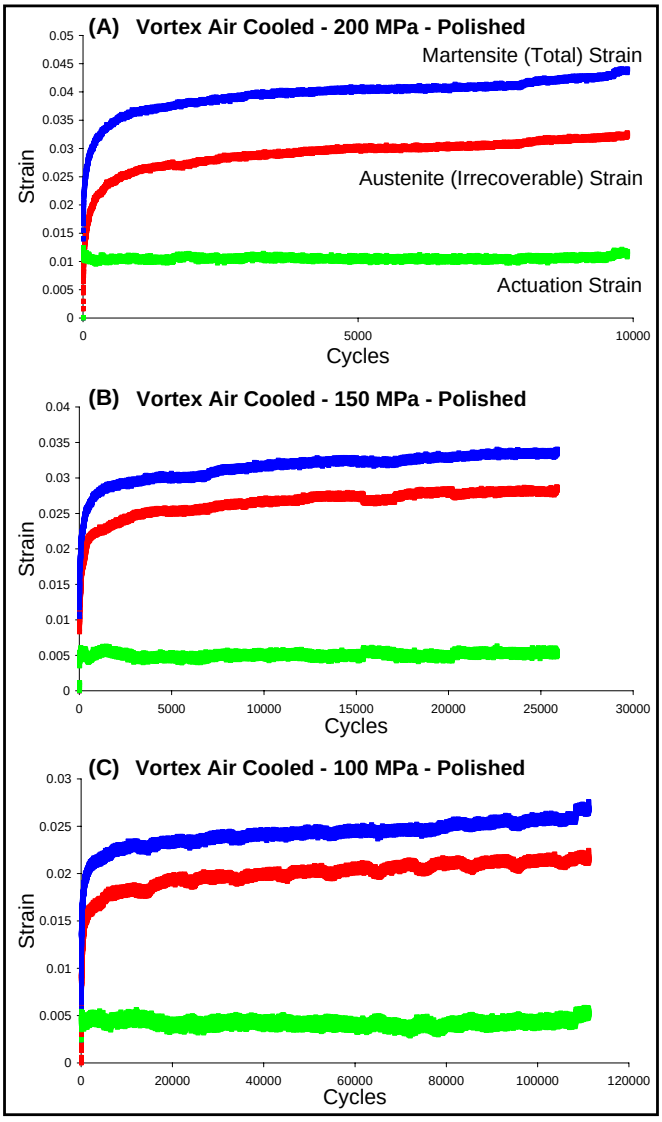

Fig. 21. Vortex air cooled transformation induced fatigue test results for (A) 200 MPa constant load, (B) 150 MPa load and (C) 100 MPa load

corresponds to the total strain in the system (irrecoverable + actuation + thermal) and austenitic strain represents the total irrecoverable strain in the system(ε^I), as shown by equation 2.4. The actuation strain is the difference between the strain in martensite and the strain in austenite, this was shown by equation 2.3. It is observed that the actuation strain remains constant throughout the life of the actuator, as seen in both sets of representative results. Constant stability in the actuation strain, without the need for extensive training, is not observed in NiTiCu or equiatomic NiTi actuators[26, 31]. The representative results in Fig. 20 and Fig. 21 also present the evolution of the irrecoverable strain over cycling. For all results the first 1000 cycles show a large accumulation of irrecoverable strain. After the first 1000 cycles, however, the accumulated irrecoverable strain per cycle stabilizes and shows very little accumulation until failure. When comparing the results from different applied stress levels it is observed that as the applied load increases, so does the actuation strain and the total irrecoverable strain. Also, as the applied load increases, the cycles to failure decreases. Finally, it is noted that the fatigue lives in Fig. 21 are longer than the fatigue lives in Fig. 20 for the same applied loads, which suggests that there is an effect from the test environment. The effects of test environment will be discussed later in this chapter.

B. Influence of Surface Finish on Transformation Induced Fatigue

All results presented in this section are from tests performed in the fatigue test frame with the liquid (ethylene-glycol) cooled environment. Two sets of specimens were studied, polished and as-received. The as-received specimens were unpolished with a rough oxide layer, a recast layer and a heat affected zone covering all surfaces. The polished specimens had a mirror quality surface finish with all oxide and recast layers

removed. All specimens had the same cross sectional area, as described in Chapter 2.

In Fig. 22, the cycles to failure compared to applied stress are presented for both polished and as-received specimens. From this plot it can be observed that the polished specimens have a greater fatigue life than the as-received specimens. Also, regardless of surface finish, the fatigue life decreases as the applied stress increases.

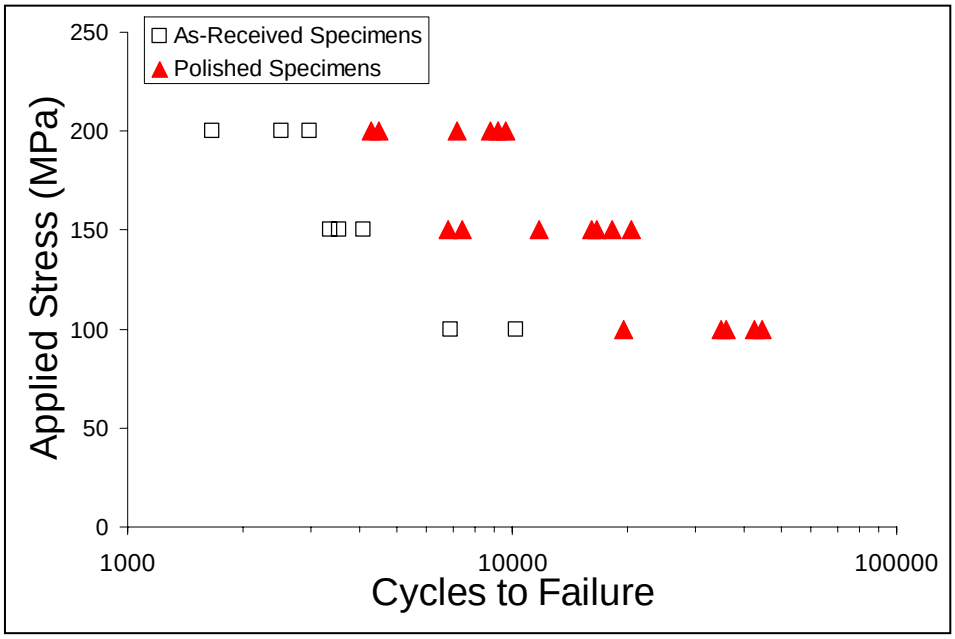

Fig. 22. Transformation induced fatigue life vs. applied stress for as-received and polished specimen tests

Table V presents the average fatigue life of the specimens tested at each applied stress level. This table shows that the average fatigue life for the polished specimens is three to four times longer than that of the as-received specimens. The response of the material is clearly affected by the rough, brittle and cracked oxide/recast layer, as would be expected.

Table V. Average fatigue life of as-received vs. polished specimens

Stress MPa (ksi)	As-received Tests	Polished Tests
200 (29.00)	2384±672	7268±2369
150 (21.75)	3676±396	13887±5306
100 (14.50)	8567±2304	35562±9854

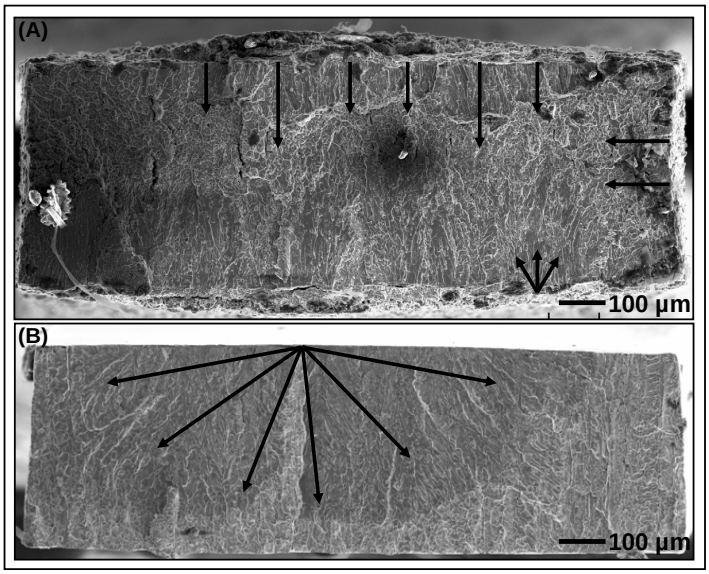

Fig. 23. Fracture surfaces of (A) an as-received specimen (B) a polished specimen[31]

Figure 23 presents the facture face surface of an as-received specimen (A) and a polished specimen (B), both tested under the same conditions. It is observed that the as-received specimen has several cracks initiating from different surface locations. It is these multiple cracks, initiating from the surface layer, that were identified as the cause of premature failure in the as-received specimen. The polished specimen, as shown in Fig. 23 (B), shows an improved response with only one crack initiation point. The result is that the more crack initiation points there are in the material,

the shorter the fatigue life.

C. Influence of Test Environment on Transformation Induced Fatigue

In this section the effects of test enviroment are investigated. It was observed that polished specimens had a corroded surface after being tested in the liquid (ethylene-glycol) environment. The surfaces of several specimens were viewed under an scanning electron microscope (SEM) and one representative example is shown in Fig. 24. By performing resistive Joule heating in a liquid, the liquid on the surface of the specimen was transformed into an electrolyte every time electric current passed through the specimen. The electrolyte reacted with the surface of the specimen and created a brittle surface layer, which then cracked easily during actuation. The corrosion caused by the electrolyte on the specimen surface can be seen in Fig. 24 (B). From

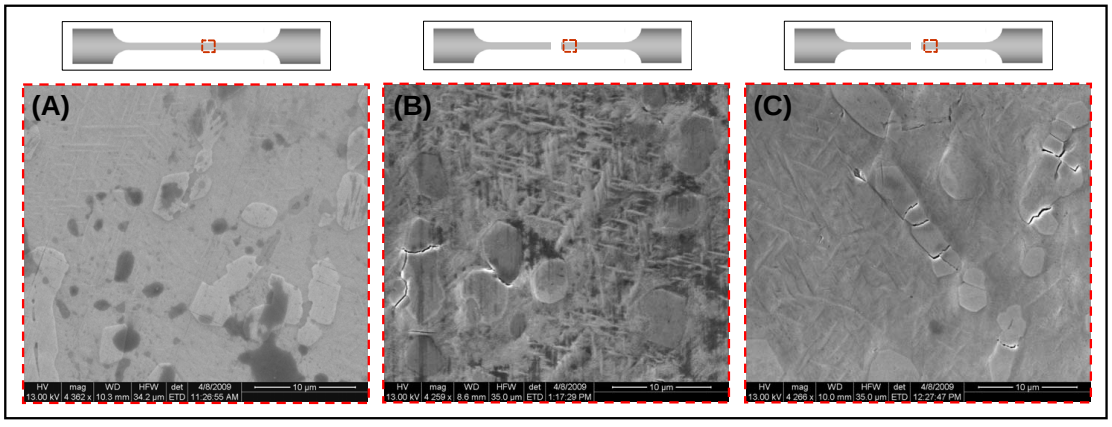

Fig. 24. Polished specimen surface (A) before testing, (B) after testing in liquid and (C) after testing in gaseous nitrogen/vortex cooled air[31]

this observation it was determined that a non-corrosive testing environment needed to be implemented. The chosen environment was gaseous nitrogen to allow for a

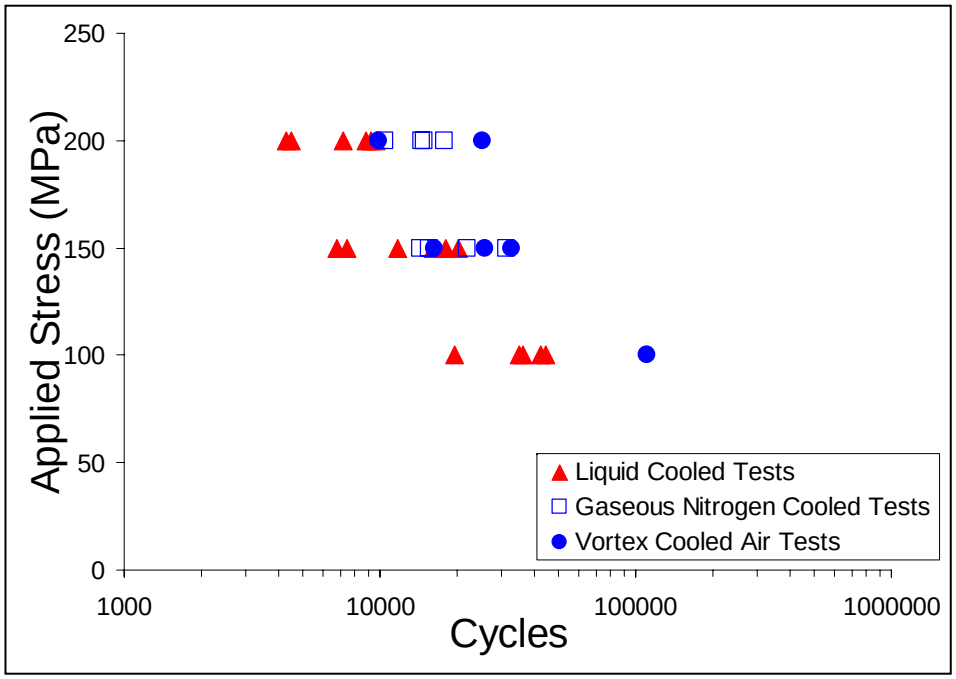

Fig. 25. Transformation induced fatigue life vs. applied stress for all polished specimens

cooler test environment, therefore comparable cycle times to the liquid cooling could be achieved. In this way, the only variable that changed from the orginal test frame to the new test frame was the cooling medium. A cheaper method than gaseous nitrogen cooling was eventually implemented (vortex cooled air) for non-corrosive testing and was shown to give comparable results.

All test results presented in this section are for specimens that have been polished. Figure 25 presents the cycles to failure compared to applied stress for liquid cooled specimens, gaseous nitrogen cooled specimens and vortex air cooled specimens. From this set of results it can be seen that the gaseous nitrogen and vortex cooled tests exhibited similar fatigue life results. The non-corrosive cooling conditions also demonstrated an improved fatigue life over the liquid cooling conditions. The aver-

Table VI. Average fatigue life of all polished specimens

Stress MPa (ksi)	Liquid Tests (Lower Bound)	GN_2/Vortex Tests (Lower Bound)
200 (29.00)	7268±2369	15473±5643
150 (21.75)	13887±5306	22576±7579
100 (14.50)	35562±9854	111180±0

age fatigue life test results are shown in Table VI. It can be seen that testing in a non-corrosive environment increased the fatigue life two to three times that of testing in a corrosive environment. Figure 24 (C) shows a representative SEM micrograph of a gaseous nitrogen/vortex air cooled test specimen. When compared to the liquid cooled specimen (B), the gaseous nitrogen/vortex air cooled specimen (C) is nearly as clean as the untested polished specimen (A); this indicates that the gaseous nitrogen environment is non-corrosive. The reason that the corrosive environment tested specimens failed before the non-corrosive environment tested specimens is that the corrosion created a brittle layer which cracked easily and, as seen with the unpolished specimens the more cracks that are initiated in the material the shorter the fatigue life. The specimens tested in a non-corrosive environment did not develop this brittle, easily cracked layer; had less crack initiation points and a longer fatigue life.

The actuation strain versus the applied stress is presented in Fig. 26. It is observed that the actuation strain is not affected by the test environment and that it increases as the applied stress increases; this response has been observed for $Ni_{60}Ti_{40}$ previously[34]. While this increase appears to be linear over the applied stresses studied here, this is not the case. The more stress that is applied to the actuator the more self-accommodated martensite that is reoriented parallel with the loading direction. This reorientation of self-accommodated martensite will saturate at some

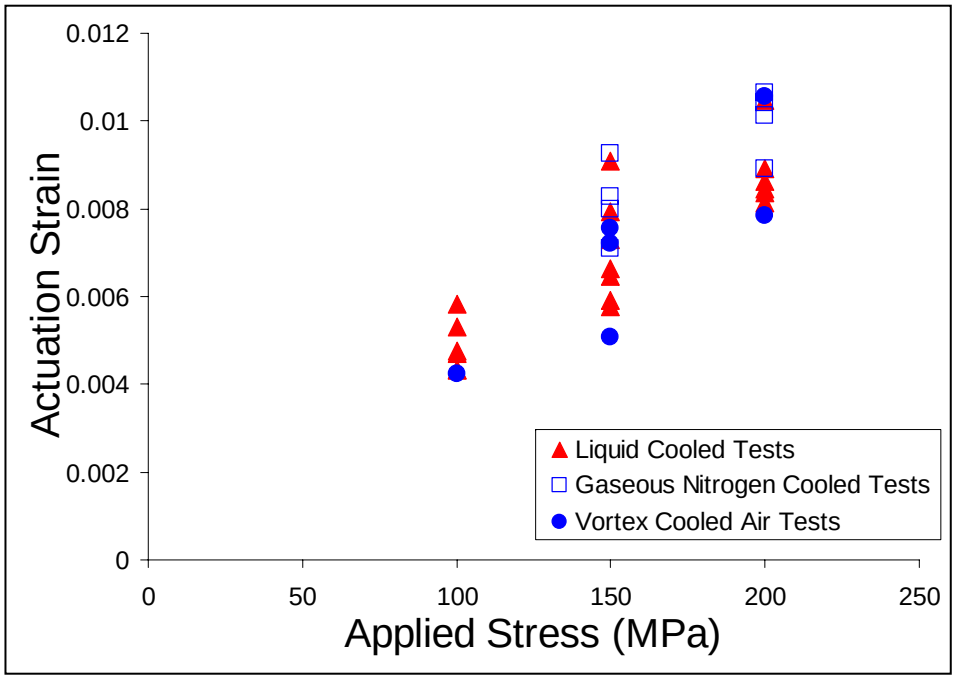

Fig. 26. Actuation strain vs. applied stress for all polished specimens

applied stress and the increase in actuation strain will no longer be observed. For this material, the martensite reorientation saturation results in an actuation strain of 1.4%.

In Fig. 27 (A) the total irrecoverable strain at failure plotted versus the applied stress is presented. From this plot it is observed that as the applied stress on the actuators increases the total irrecoverable strain at failure increases. It can also be noted that the test environment does not have an effect on the total irrecoverable strain at failure. Figure 27 (B) presents the total irrecoverable strain at failure versus the number of cycles at failure. When comparing the irrecoverable strain to the number of cycles it is difficult to make any correlation. To explain why there is no apparent correlation Fig. 25 and Fig. 27 (A) need to be more closely studied. In Fig. 25 cycles to failure increase as applied stress decreases, however there is a

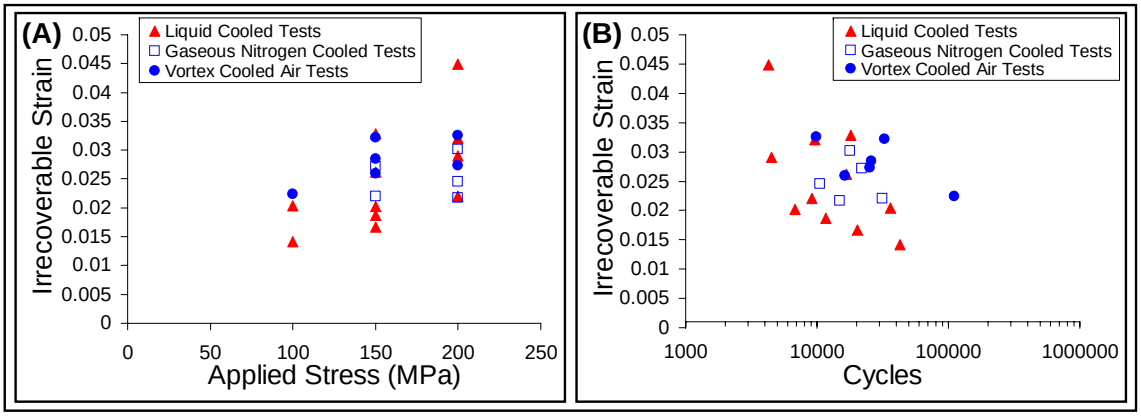

Fig. 27. Irrecoverable strain at failure for polished specimens vs. (A) applied stress and (B) cycles at failure

spread in the fatigue life at each applied stress. For example, several actuators at 200 MPa have longer fatigue lives than actuators tested at 150 MPa and several actuators at 150 MPa outperformed actuators at 100 MPa. Based on the trend that irrecoverable strain increases as applied stress increases combined with the spread in the fatigue lives leads to a lack or correlation for irrecoverable strain and cycles at failure. Furthermore, there is a similar spread in the applied stress versus total irrecoverable strain in Fig. 27(A). For a given applied stress the total irrecoverable strain at failure has a range of 2%. This spread in the irrecoverable strain combined with the spread in cycles at failure compounds the lack of correlation observed in Fig. 27 (B).

D. Microstructural Observations

As noted in the previous section, a spread in the data was observed in Fig. 25 and Fig. 27. While some experimental variation is expected, the dispersion of test results was quite large. For example, the standard deviation of fatigue lives for all polished

specimens ranged from ±30% to ±35%. Similarly, irrecoverable strain at failure at different applied stress levels had standard variations of ±20% to ±30%. To determine the cause for such dispersion in results, a study of the microstructure was performed. A thorough study on the failure mechanisms of this material is provided in a colleagues work[31] and will be discussed briefly in this section.

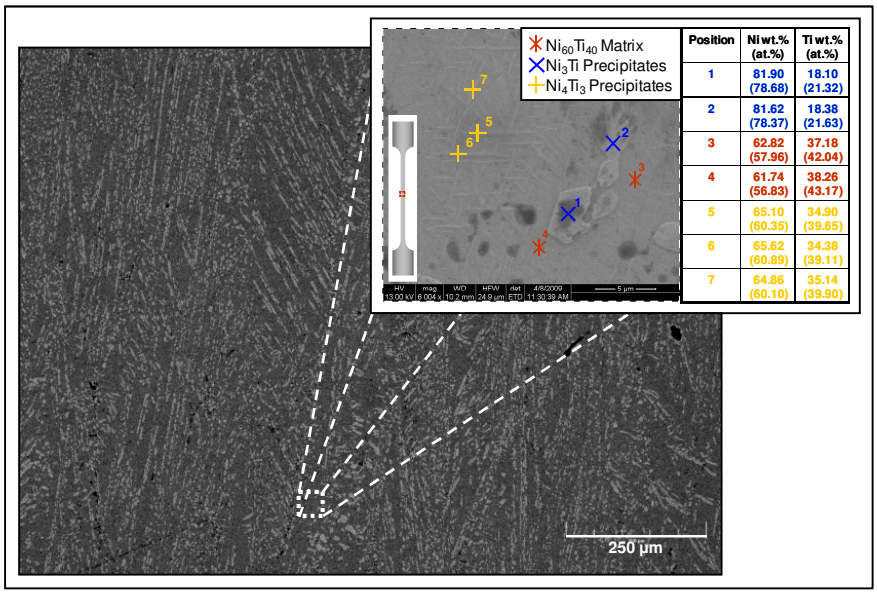

Position	Ni wt.% (at.%)	Ti wt.% (at.%)
1	81.90 (78.68)	18.10 (21.32)
2	81.62 (78.37)	18.38 (21.63)
3	62.82 (57.96)	37.18 (42.04)
4	61.74 (56.83)	38.26 (43.17)
5	65.10 (60.35)	34.90 (39.65)
6	65.62 (60.89)	34.38 (39.11)
7	64.86 (60.10)	35.14 (39.90)

Fig. 28. Characterization of precipitates using SEM[31]

The goal in processing Ni-rich NiTi SMAs for use as actuators was to use Ni-rich precipitates to stabilize the material's cyclic response, similar to precipitation hardening in conventional alloys. The test results previously presented in Fig. 20 and Fig. 21 show that the precipitation hardening has an effect on performance; the actuation strain for the material is shown to be constant from the beginning to the end of testing and the total irrecoverable strain in the system is limited to less than 3%. In comparison, equiatomic NiTi, which does not have precipitation hardening,

reaches irrecoverable strains of 5-10%. Also, as previously noted for equiatomic NiTi, as irrecoverable strain increases over cycling the actuation strain correspondingly decreases. This is where precipitation hardening demonstrates its value for SMA actuators; actuation strain does not degrade as irrecoverable strain accumulates in Ni-rich NiTi SMAs, and the accumulation of irrecoverable strain is limited to a small amount. For this material two of the primary Ni-rich precipitates have been identified by SEM characterization, as presented in Fig. 28. The needle-like precipitates are Ni_4Ti_3, which assist transformation. The large bulky precipitates are Ni_3Ti and have been shown to not improve material performance.

Initial observations of the specimen surface found the material contained an extremely large amount of the Ni_3Ti precipitates. An untested specimen surface and cross-section are presented in Fig. 29. It can be observed that not only are there

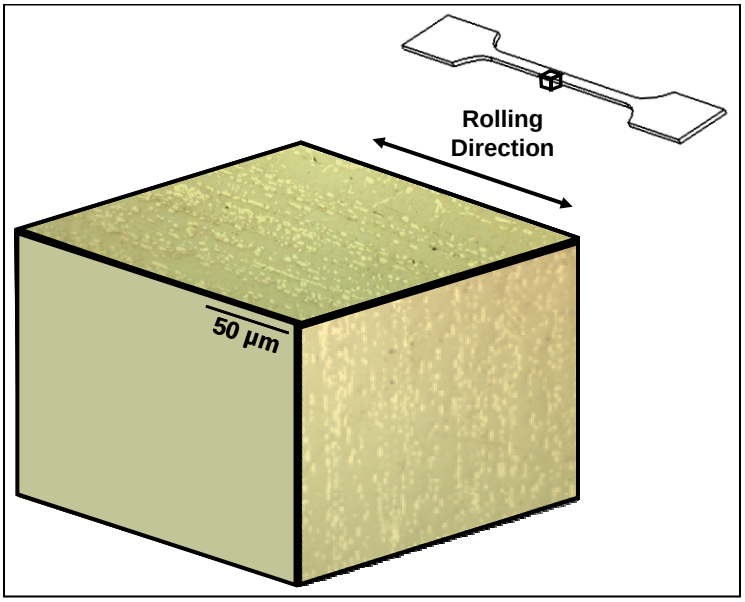

Fig. 29. Untested specimen surface and cross-section

a lot of Ni_3Ti precipitates, but they are also unevenly distributed with clustered bands in line with the rolling direction. Upon examining the cross-section of the specimen it can be seen that these bands of precipitates go through the thickness of the specimen as well. A post-failure specimen surface was then analyzed and is shown in Fig. 30. From this examination, it can be seen that the clustered Ni_3Ti precipitates

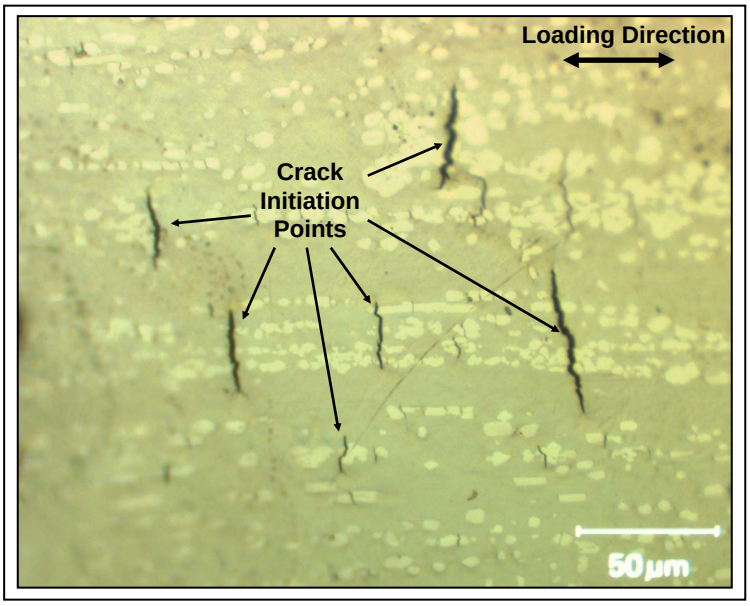

Fig. 30. Post-failure specimen surface

are acting as crack initiation points at the material surface, with cracks propagating perpendicular to the applied load direction. Not only do these precipitates act as initiation points, but they provide a path for cracks to propagate through the test gauge thickness, ultimately leading to specimen failure, which is shown in Fig. 31. It is the non-homogeneous distribution of Ni_3Ti precipitates and small specimen cross-section that are believed to cause such a scatter in the test results. For example, if a specimen was cut from a region with a large clustering of Ni_3Ti precipitates its

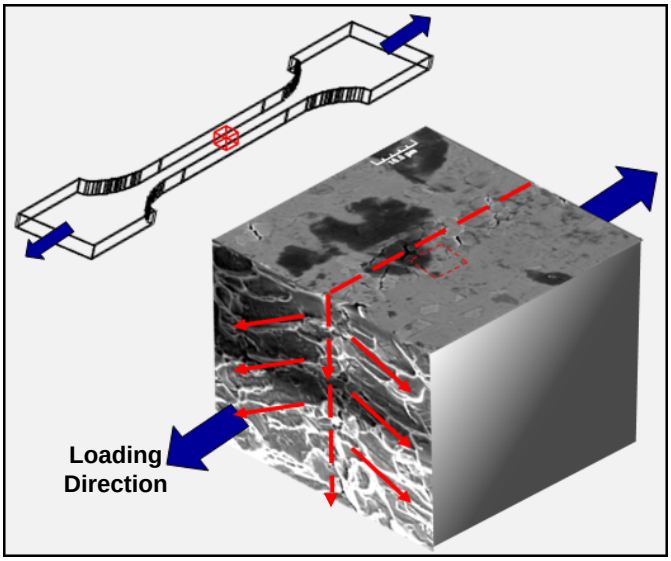

Fig. 31. Crack initiation and propagation sites[31]

fatigue life will be severely decreased and its irrecoverable strain at failure will be lower. On the other hand, if a specimen is cut from a region with less precipitates, its fatigue life will be longer and its irrecoverable strain at failure will be higher because there will be fewer crack initiation points that lead to premature failure. Due to the small size of test specimens there is a greater chance for variation in the amount of precipitates from specimen to specimen, and this will lead to a large spread in the fatigue life results.

CHAPTER IV

CONCLUSIONS AND FUTURE WORK

A. Conclusions

In this work, the first comprehensive transformation induced fatigue study of the Ni-rich SMA $Ni_{60}Ti_{40}$ (wt.%) was presented. Fatigue tests were performed for complete thermal transformation cycles from above A_f to below M_f, under various constant applied stress levels. The fatigue life and material response, including the actuation strain and irrecoverable strain, were studied. The effects of specimen surface finish and test environment on fatigue were also studied and presented in this work.

The first comparison was made between as-received and polished specimen fatigue lives. In this comparison, all specimens were tested in the fatigue test frame that implemented liquid cooling to bring the temperature of the specimens below M_f and Joule heating to raise the specimen's temperature above A_f. Next, the effects of testing environment on fatigue life were addressed. A new test frame was designed and built to have the same capabilities as the original, except for a change in the cooling medium. The new test frame used gaseous nitrogen to cool the specimens, while the old test frame used a liquid. While this new cooling method was effective, it was expensive and difficult to maintain. A new non-corrosive cooling system was implemented (vortex air cooling) and was found to perform comparably to gaseous nitrogen. Finally, a study of specimen microstructure was performed in an effort to determine the cause of crack initiation, crack propagation, and specimen failure[31].

In the fatigue life comparison of as-received and polished specimens, it was found that the polished specimens had longer fatigue lives than those of the as-received specimens. On average, the polished specimens had fatigue lives that were three to

four times the fatigue lives of as-received specimens. As with conventional metal fatigue, fatigue life increases as surface quality improves. The environment also has an effect on the transformation induced fatigue, and this study found that the liquid cooling created a corrosive environment, where as gaseous nitrogen and vortex cooling were non-corrosive environments. Gaseous nitrogen and vortex cooled test results were shown to perform similarly and had fatigue lives that were twice as long as specimens tested in the liquid cooled environment. Despite the difference in test environments, all tests showed a decrease in fatigue life as applied stress increases. For example, the transformation induced fatigue polished specimens in a non-corrosive environment at 200 MPa had an average fatigue life of 14400 actuation cycles, at 150 MPa the average fatigue life was 20800 cycles and at 100 MPa it was 111000 cycles. The test environment was also found to not have an effect on either actuation strain or total irrecoverable strain. Finally, it was observed for all fatigue results that there was a standard deviation in the data of $\pm 30\%$ to $\pm 35\%$.

To determine the cause of this spread, the micrstructure of the pre/post-failure specimens was studied, and it was determined that Ni_3Ti precipitates created during the material processing and subsequent heat treatments were ultimately leading to specimen failure. These precipitates were unevenly distributed throughout the material and tended to be in clusters that were observed to go through the thickness of tested specimens. Cracks would initiate on the surface of the specimens within these clustered precipitates and then propagate through the thickness. Due to the small size of the specimens, the volume fraction of precipitates is assumed to vary from specimen to specimen. This variation of precipitate volume fraction may cause the large spread observed in the fatigue life results.

This work has shown that $Ni_{60}Ti_{40}$ has stable actuation and limited irrecoverable strain at various applied loads. In exhibiting these two properties this material can

be accepted as a viable actuator for aerospace applications.Also, as long as applied loads are $\leq$100 MPa (14.5 ksi) actuators have shown fatigue lives of up to 111000 actuation cycles in non-corrosive environments. This shows that the material can be implemented into aerospace structures and perform reliably for operational lifetime of the aircraft.

Finally, this study took the initial steps in creating a repeatable test methodology for SMA actuator testing. To test small SMA actuators to get bulk material property these actuators must be polished to ensure they do not have any surface effects. Testing should be performed in a non-corrosive environment and vortex cooling has been shown to be non-corrosive and just as effective as gaseous nitrogen cooling. Vortex cooling was also cheaper and easier to maintain.

B. Future Work

While the fatigue life of $Ni_{60}Ti_{40}$ was extensively studied in this work, there is much remaining to study in the area of transformation induced fatigue of SMAs. Achieving a standard methodology for testing remains the ultimate goal. Steps that can now be take include testing larger specimens and conducting spring-bias fatigue testing. Testing specimens that are larger than the specimens used in this study will help to determine if there is a size effect. This includes a better average distribution of Ni_3Ti precipitates from specimen to specimen. Conducting spring-bias fatigue testing is important because most SMA actuator applications do not see constant stress, instead these actuators see a variation in stress throughout the actuation process. Thus, to better predict the fatigue life of true actuator systems testing should be performed against a spring-bias load and not a constant load. Finally, while $Ni_{60}Ti_{40}$ shows great potential as a stable actuator, recent research has shown

that the Ni_3Ti precipitates found in the matrix are the driving force behind the material failure[31]. To improve material performance, a new processing technique or heat treatment meathod needs to be developed for this material that limits the size and amount of the Ni_3Ti precipitates. Testing also needs to be performed on Ni-rich SMAs with a lower Ni content, such as $Ni_{57}Ti_{43}$ or $Ni_{56}Ti_{44}$ (wt.%) to see how the material performs and to see if a median can be found between limiting precipitate driven failure, while still keeping stable actuator performance.

REFERENCES

[1] G. B. Kauffman, I. Mayo, The story of nitinol: The serendipitous discovery of the memory metal and its applications, The Chemical Educator 2 (2) (1996) 1–21.

[2] T. Duerig, A. Pelton, D. Stoeckel, An overview of nitinol medical applications, Material Science and Engineering A273-275 (1999) 149–160.

[3] N. B. Morgan, Medical shape memory alloy applications - the market and its products, Material Science and Engineering A378 (2004) 16–23.

[4] D. J. Hartl, D. C. Lagoudas, Aerospace applications of shape memory alloys, Proceedings of the Institution of Mechanical Engineers, Part G: Journal of Aerospace Engineering 221 (4) (2007) 535–552.

[5] J. N. Kudva, Overview of the darpa smart wing project, Journal of Intelligent Material Systems and Structures 15 (2004) 261–267.

[6] D. M. Pitt, J. P. Dunne, E. V. White, Sampson smart inlet SMA powered adaptive lip design and static test, American Institute of Aeronautics and Astronautics 1359 (2001) 1–11.

[7] J. H. Mabe, R. T. Ruggeri, E. Rosenzweig, C. Yu, Nitinol performance characterization and rotary actuator design, in: E. H. Anderson (Ed.), Smart Structures and Materials 2004: Industrial and Commercial Applications of Smart Structures Technologies, Vol. 5388, SPIE, 2004, pp. 95–109.

[8] J. H. Mabe, F. T. Calkins, G. W. Butler, Boeing's variable geometry chevron, morphing aerostructure for jet noise reduction, in: 47th

AIAA/ASME/ASCE/AHS/ASC Structures, Structural Dynamics, and Materials Conference, Vol. 2142, American Institue of Aeronautics and Astronautics, Newport, RI, 2006, pp. 1–19.

[9] D. J. Hartl, P. K. Kumar, L. G. Machado, D. C. Lagoudas, B. Kiefer, P. Popov, P. B. Entchev, M. A. Qidwai, Shape Memory Alloys: Modeling and Engineering Applications, Springer, 2007.

[10] K. N. Melton, O. Mercier, Fatigue of niti thermoelastic martensites, Acta Metallurgica 27 (1978) 137–144.

[11] H. Tobushi, S. Yamada, T. Hachisuka, A. Ikai, K. Tanaka, Thermomechanical properties due to martensitic and r-phase transformations on tini shape memory alloy subjected to cyclic loadings, Smart Material Structures 5 (1996) 788–795.

[12] H. Tobushi, T. Hackisuka, S. Yamada, P. Lin, Rotating-bending fatigue of a tini shape-memory alloy wire, Mechanics of Materials 26 (1997) 35–42.

[13] H. Tobushi, T. Nakahara, Y. Shimeno, T. Hashimoto, Low-cycle fatigue of tini shape memory alloy and formulation of fatigue life, ASME 122 (2000) 186–191.

[14] Y. Furuichi, H. Tobushi, T. Ikawa, R. Matsui, Fatigue properties of a tini shape-memory alloy wire subjected to bending with various strain ratios, Proceedings of the Institution of Mechanical Engineers, Part L: Journal of Materials: Design and Applications 217 (2) (2003) 93–99.

[15] A. Pelton, X. Y. Gong, T. W. Duerig, Fatigue testing of diamond-shaped specimens, in: T. W. Duerig, A. Pelton (Eds.), Proceedings of the International Conference on Shape Memory and Superelastic Technologies, 2003, pp. 293–302.

[16] G. S. P. Cheung, B. W. Darvell, Fatigue testing of a niti rotary instrument. part 1: Strain-life relationship, International Endodontic Journal 40 (2007) 612–618.

[17] W. Predki, M. Klonne, A. Knopik, Cyclic torsional loading of pseudoelastic niti shape memory alloys: Damping and fatigue failure, Materials Science and Engineering A 417 (2006) 182–189.

[18] D. Fugazza, Experimental investigation on the cyclic properties of superelastic niti shape-memory alloy wires and bars, Ph.D. thesis, Universita degli Studi di Pavia (August 2005).

[19] M. Dolce, D. Cardone, Fatigue resistance of sma-martensite bars subjected to flexural bending, International Journal of Mechanical Sciences 47 (2005) 1693–1717.

[20] A. M. Figueiredo, P. Modenesi, V. Buono, Low-cycle fatigue life of superelastic niti wires, International Journal of Fatigue 31 (4) (2009) 751–758.

[21] J. Mabe, R. T. Ruggeri, E. Rosenzweig, C. Yu, Nitinol performance characterization and rotary actuator design, in: E. H. Anderson (Ed.), Smart Structures and Materials 2004: Industrial and Commercial Applications of Smart Structures Technologies, Vol. 5388, 2004, pp. 95–109.

[22] J. L. Proft, K. N. Melton, T. W. Duerig, Transformation cycling of ni-ti and ni-ti-cu shape memory alloys, Materials Research Society International Meeting on Advanced Materials 9 (1989) 159–164.

[23] D. C. Lagoudas, D. A. Miller, L. Rong, P. K. Kumar, Thermomechanical fatigue of shape memory alloys, Smart Materials and Structures 18 (2009) 1–12.

[24] O. W. Bertacchini, D. C. Lagoudas, E. Patoor, Fatigue life characterization of shape memory alloys undergoing thermomechanical cyclic loading, in: D. C. Lagoudas (Ed.), Proceedings of the Smart Structures and Materials 2003, Vol. 5053, 2003, pp. 612–624.

[25] C. J. de Araujo, M. Morin, G. Guenin, Fatigue behavior of ti-ni-cu thin wires sme, Journal de Physique IV 7 (5) (1997) C5.501–C5.506.

[26] J. H. Mabe, R. Ruggeri, F. T. Calkins, Characterization of nickel-rich nitinol alloys for actuator development, in: The International Conference on Shape Memory and Superelastic Technologies, Pacific Grove, CA, 2006.

[27] N. B. Morgan, C. M. Friend, A review of shape memory stability in niti alloys, Journal de Physique IV 11 (2001) Pr8–325–Pr8–332.

[28] K. Gall, N. Yang, H. Sehitoglu, Y. I. Chumlyakov, Fracture of precipitated niti shape memory alloys, International Journal of Fracture 109 (2001) 189–207.

[29] C. C. Wojcik, Aging effects in nickel rich ni-ti alloys, Tech. rep., Wah Chang, an Allegheny Technologies Company (2004).

[30] D. C. Lagoudas, D. A. Miller, L. Rong, P. K. Kumar, Thermomechanical fatigue of shape memory alloys, Smart Material Structures 18 (2009) 1–12.

[31] O. W. Bertacchini, Characterization and modeling of transformation induced fatigue of shape memory alloy actuators, Ph.D. thesis, Texas A&M University, College Station, TX (August 2009).

[32] H. C. Lin, K. M. Lin, I. S. Cheng, The electro-discharge machining characteristics of TiNi shape memory alloys, Journal of Materials Science 36 (2001) 399–404.

[33] W. Theisen, A. Schuermann, Electro discharge machining of nickel-titanium shape memory alloys, Materials Science and Engineering 378 (2004) 200–204.

[34] D. J. Hartl, D. C. Lagoudas, Characterization and 3-d modeling of ni60ti sma for actuation of a variable geometry jet engine chevron, in: M. Tomizuka, C. Yun, V. Giurgiutiu (Eds.), Sensors and Smart Structures Technology for Civil, Mechanical, and Aerospace Systems 2007, Vol. 6529, SPIE, 2007.

APPENDIX A

STEP-BY-STEP POLISHING PROCEDURE

STEP 1: SPECIMEN SIDES (Thickness face of the test gauge)

1. Place specimen into the first set of custom grips, so that the specimen side extends out (SIDE 1).
2. Place specimen holder down on the Dremel stand so that SIDE 1 is perpendicular to the aluminum oxide grinding head.
3. Turn the Dremel on to level 3, with one hand use a squirt bottle to spray water where the grinding head meets SIDE 1 and with the other hand slowly and gently move SIDE 1 back and forth along the grinding head until SIDE 1 is flush with the grips.
4. Take the specimen out of the grips and rotate it horizontally so that the left side of the specimen is on the right and the right on the left always remembering to keep SIDE 1 up, close the grips again.
5. Repeat step 3 to ensure an even polish on SIDE 1.
6. Switch the grinding head to the rubber polishing head and repeat steps 3-5 for SIDE 1.
7. Place the specimen into the second set of custom grips, so that the side opposite SIDE 1 is facing out of the grips (SIDE 2).
8. Repeat steps 2-6 for SIDE 2.

STEP 2: SPECIMEN FACES (Width face of the test gauge)

1. Place a specimen (sides already polished) into the custom specimen holder with two-sided tape; this is done for two specimens at a time.

2. Place the two specimen holders on opposite sides of the holder wheel. Connect the holder wheel to the RotoForce-4 arm.

3. Place 400-grit disk onto the RotoPol-31 and set the RotoForce-4 to 5 N force and counter-clockwise direction; polish for 20 seconds.

4. Change the RotoForce-4 polishing direction to the clockwise direction; polish for 20 seconds.

5. Take the holder wheel off the RotoForce-4 arm and spin the specimens around so that each specimen's left side is now the right and the right now the left; place the holder wheel back onto the polishing arm.

6. Repeat steps 3-4. By rotating the specimen around, you ensure that an even polish is achieved on each side.

7. Next, place a 1200-grit disk onto the RotoPol-31, set the RotoForce-4 for counter-clockwise spin, 5 N force, and polish for 45 seconds.

8. Change the RotoForce-4 polishing direction to the clockwise direction; polish for 45 seconds.

9. Repeat step 5.

10. Repeat steps 7-8.

11. Repeat steps 7-10 using a 2000-grit grit disk.

12. Next, place a cloth polishing disk on the RotoPol-31; use a 6 micron diamond polish. Set the RotoForce-4 to counter-clockwise spin; polish for 120 seconds.

13. Repeat step 12, setting the RotoForce-4 to a clockwise spin.

14. Repeat steps 12-13 using a 0.3 micron diamond polish.

15. Remove specimens from the custom holders and flip them so that the unpolished face is exposed, secure them into the custom holders with two-sided tape and repeat steps 2-14.

VITA

Justin Ryan Schick is the first of three sons, his brothers are Josh and Jarred. Justin was born in Sparks, Nevada. His family moved from Nevada to Kansas City, Missouri when he was 9 and then to Mandeville, Louisiana when he was 14. It was in Louisiana where Justin attended St. Paul's High School. Once he graduated, he attented Texas A&M University where he received his B.S. in Aerospace Engineering in December of 2007. Justin continued on to graduate school at Texas A&M in January of 2008. He will graduate with a M.S. in Aerospace Engineering in December of 2009. The work Justin has done has been under the guidance of Dr. Dimitris C. Lagoudas. Justin's research interests include the fatigue of SMAs and their application for thermomechanical actuator applications. A complete resume may be found at http://smart.tamu.edu. Justin can be reached through the Texas A&M Aerospace Department:

Aerospace Engineering
c/o Dr. Dimitris Lagoudas
Texas A&M Unversity College Station, TX 77843-3141
His email address is Schick13@tamu.edu.